

Predicting survival and trial outcome for anti-PDL1 in non-small cell lung cancer using tumor and blood markers kinetics

Sébastien Benzekry¹✉, Mélanie Karlsen¹, Célestin Bigarré¹, Abdessamad El Kaoutari¹, Bruno Gomes², Martin Stern³, Ales Neubert⁴, Rene Bruno⁵, François Mercier⁶, Suresh Vatakuti⁷, Peter Curle⁸, Candice Jamois⁹

¹COMPUTational pharmacology and clinical Oncology Department, Inria Sophia Antipolis–Méditerranée, Cancer Research Center of Marseille, Inserm UMR1068, CNRS UMR7258, Aix Marseille University UM105, Marseille, France; ²Pharma Research and Early Development, Early Development Oncology, Roche Innovation Center Basel, Switzerland; ³Pharma Research and Early Development, Early Development Oncology, Roche Innovation Center Zurich, Switzerland; ⁴Pharma Research and Early Development, Data & Analytics, Roche Innovation Center Basel, Switzerland; ⁵Modeling and Simulation, Clinical Pharmacology, Genentech Research and Early Development, Marseille France; ⁶Modeling and Simulation, Clinical Pharmacology, Genentech Research and Early Development, Roche Innovation Center Basel; ⁷Pharma Research and Early Development, Predictive Modeling and Data Analytics, Roche Innovation Center Basel, Switzerland; ⁸Inovigate, Basel, Switzerland; ⁹Pharma Research and Early Development, Translational PKPD and Clinical Pharmacology, Roche Innovation Center Basel, Switzerland

✉ For correspondence: sebastien.benzekry@inria.fr

Present address: COMPO team, Pharmacy faculty
27 Bd Jean Moulin
13385 Marseille, FRANCE

Data availability: Qualified researchers may request access to individual patient level data through the clinical study data request platform (<https://vivli.org/>). Further details on Roche's criteria for eligible studies are available here (<https://vivli.org/members/ourmembers/>). For further details on Roche's Global Policy on the Sharing of Clinical Information and how to request access to related clinical study documents, see here <https://www.roche.com/innovation/process/clinical-trials/data-sharing/>.

Funding: This work was sponsored by the Roche Pharma Research and Early Development (pRED) One-D Modeling and Simulation Digital Initiative. It also benefited from funding from ITMO Cancer AVIESAN and French Institut National du Cancer (grant #19CM148-00)

Competing interests: The authors declare the existence of a financial competing interest

Abstract

Current predictive models of survival typically use baseline or tumor kinetics data. We propose a novel kinetics-machine learning (kML) integrative model of overall survival following anti-PDL1 treatment in non-small cell lung cancer. It incorporates eleven baseline markers and four on-treatment blood markers: albumin, C-reactive protein, lactate dehydrogenase and neutrophils. The kML model was developed on three phase 2 trials (862 patients) and validated on a phase 3 trial (553 patients). It outperformed the current state-of-the-art for individual predictions with a test set c-index of 0.79, a 12-months AUC of 0.86 and a hazard ratio of 25.2 (95% CI: 10.4 – 61.3, $p < 0.0001$) for identification of long-term survivors. kML was also able to anticipate the success of the phase 3 trial by utilizing only 25 weeks of on-study data. It constitutes a valuable approach to support personalized medicine and drug development.

Introduction

Lung cancer is the leading cause of cancer death worldwide¹, with non-small cell lung cancer (NSCLC) being the most prevalent type, representing 80% – 85% of case². Immune-checkpoint inhibitors (ICI) (e.g., atezolizumab (ATZ)) have led to significant improvements in survival rates for pa-

It is made available under a [CC-BY-NC-ND 4.0 International license](https://creativecommons.org/licenses/by-nc-nd/4.0/) .

39 tients with advanced cancers such as NSCLC^{3,4}. However, there is still a large variability in clinical
40 response and progression eventually occurs in a majority of patients⁵. Additionally, drug devel-
41 opment in immuno-oncology is highly challenging, with a 95% attrition rate⁶. Current approaches
42 for go/no-go decisions are based on interim endpoints (e.g., progression-free survival, overall re-
43 sponse rate) that have often been found to be poor predictors of the primary endpoint of most
44 clinical trials in oncology, overall survival (OS)⁷. This calls for better surrogate markers at interim
45 analyses. Altogether, there is a need for better and validated predictive models of OS for both
46 personalized health care (individual predictions) and drug development (trial predictions).

47 Currently, PDL1 expression is the only routine biomarker used for NSCLC patients^{5,8} despite
48 being controversial^{9,10}. Tumor mutational burden^{8,11,12} and transcriptomic data^{5,13,14} have also
49 been investigated but did not reach clinical practice. Here we posit that such static and single
50 marker approach is intrinsically limited and that substantial additional predictive performances
51 could be gained by: 1) using multi-modal integrative analyses relying on a combination of markers
52 and machine learning algorithms^{5,12,14,15} and 2) including dynamic markers obtained from early
53 on-treatment data^{15,16}. The nonlinear mixed-effects (NLME) modeling approach is well suited for
54 the latter¹⁷, and tumor kinetics (TK) model-based metrics have been shown to carry significant
55 predictive value for OS in oncology, including ATZ monotherapy in advanced NSCLC¹⁸⁻²⁰. The first
56 main novelty of the current study is to establish the predictive value of model-based parameters
57 of simple blood markers kinetics (BK), in addition to TK.

58 The second main novelty is to apply machine learning (ML) algorithms, increasingly used in
59 biology and medicine²¹ but only rarely for TK-OS modeling²², instead of classical survival mod-
60 els. Extensions of classical ML models to survival data have been proposed (e.g., random survival
61 forests²³), but their actual superiority over standard approaches remains controversial²⁴.

62 Here, we coupled the strengths of NLME modeling with ML to derive a predictive model of
63 OS from baseline and on-treatment data, called kinetics-Machine Learning (kML). We leveraged
64 extensive training and testing datasets to achieve robust results. Subsequently, we tested the
65 operational predictive capabilities of kML in two relevant scenarios: 1) individual prediction of OS
66 and 2) prediction of the outcome of a phase 3 trial from early on-study data.

67 **Methods**

68 **Data**

69 For both training and external validation (testing) sets, patients from French centers were excluded
70 for legal reasons ($N = 118$, not included in the numbers above). The training set comprised the
71 FIR (NCT01846416)²⁵, POPLAR (NCT01903993)³ and BIRCH (NCT02031458)²⁶ phase 2 clinical trials.
72 The testing set was the atezolizumab arm of the OAK phase 3 trial (NCT02008227)²⁷. These studies
73 were conducted in accordance with the Declaration of Helsinki after approval by institutional review
74 boards or independent ethics committees. All patients provided written informed consent.

75 The outcome considered was overall survival (OS), defined as the time between treatment start
76 and death or last follow-up, in which case the data was right-censored. The median follow-up was
77 35.2 months (95%CI:34.5–35.7) in the training set and 26.8 months (95%CI:26.3–27.5) in the test set.

78 **Preprocessing**

79 **Baseline data**

80 The baseline data consisted of 63 variables spanning demographic and biological data, clinical in-
81 formation and disease status (see Appendix 1—figure 1–4 for a description of the main variables).
82 PD-L1 expression on tumor cells was measured by immunohistochemistry or quantitative poly-
83 merase chain reaction, with four possible levels (0: < 1%; 1: $\geq 1\%$; 2: $\geq 5\%$ and 3: $\geq 50\%$)³. We refer
84 to the above-mentioned identifiers and references for further details on the other variables. Data
85 were measured in accordance to the studies principles.

It is made available under a [CC-BY-NC-ND 4.0 International license](https://creativecommons.org/licenses/by-nc-nd/4.0/) .

86 Missing values (1.6% total, maximum 12% in one variable) were imputed with median for nu-
87 meric variables and mode for categorical variables, learned on the training set, even when apply-
88 ing the model to the testing set. Following preprocessing, all numeric variables were centered and
89 scaled. Means and standard deviations was learned on the train and carried to the test set.

90 Dimensionality reduction for RNAseq

91 Initial expression data from RNAseq consisted of 715 patients and 58,311 transcripts. The first step
92 of data filtering removed all transcripts with less than 10 read counts for all patients, then selected
93 genes with highest variability between patients (top 15,000 transcripts most variable). Then, data
94 were normalized using upper quartile normalization which consisted in dividing each read count
95 by the 75th percentile of the read counts of the corresponding sample and the final expression
96 values were \log_2 transformed. Subsequently, a univariable Cox regression model was employed
97 to statistically assess the correlations between the expression levels of the transcripts and overall
98 survival. Bonferroni correction was used to adjust p-values from multiple univariate tests. This
99 step was performed using the `RegPara11e1` R package. We selected transcripts with high predictive
100 values using following criteria: adjusted log rank < 0.01 and $HR < 0.85$ or $HR > 1.2$. The remaining
101 transcripts were used to perform a bootstrap Lasso Cox regression²⁸ with cross-validation using
102 mainly the `glmnet` R package. Finally, the smallest number of transcripts with best predictive model
103 (highest c-index) was selected for further analysis.

104 Tumor kinetics (TK)

105 Patients with only one baseline SLD measurement and no SLD measurement during the treatment
106 period were excluded ($N = 110$).

107 Blood markers kinetics (BK)

108 Only patients with at least two observations on-treatment, pre-cycle 5 (3 months) were considered.
109 Time points prior to treatment start were discarded. Five rules were established to exclude irrel-
110 evant data points or patients from the BK dataset. First, lower (LB) and upper (UB) physiological
111 bounds were established after discussion with a clinical oncologist. Outliers (observations outside
112 these bounds) were discarded using the following bounds: albumin, LB = 10g/l, UB = 100g/l; CRP,
113 no LB, UB = 300mg/l; LDH, LB = 50U/l, UB = 2000U/l; neutrophils, no LB, UB = 20G/l. Second,
114 duplicate time points were removed, keeping the first one recorded. Third, aberrant outliers were
115 identified. Denoting BK_n^k the value of the k-th BK at time t_n for a give patient, we excluded values
116 such that: $BK_n^k \notin (BK_{n-1}^k, BK_{n+1}^k)$, and $|BK_n^k - BK_{n-1}^k| > 3 \times sd_{BK^k}$, and $|BK_n^k - BK_{n+1}^k| > 3 \times sd_{BK^k}$,
117 where sd_{BK^k} is the standard deviation of $\{BK_n^k\}$. Fourth, for each patient, only the BK value at the
118 closest time point to treatment initiation was kept, provided this time point was no more than 40
119 days before or 10 days after treatment initiation (otherwise, patient was disregarded). Fifth, in or-
120 der to have sufficient data for Bayesian parameter estimation with early data, patients with less
121 than three data points before cycle five were removed.

122 Nonlinear mixed-effects modeling

123 Population approach

124 Statistical hierarchical nonlinear mixed-effects modeling (NLME) was used to implement a popula-
125 tion approach for the kinetic data²⁹. Briefly, denoting by $M(t; \theta)$ a structural dynamic model that
126 depends on time t and a set of parameters θ , longitudinal observations y_j^i in patient i at time t_j^i
127 were assumed to follow the observation model

$$y_j^i = M(t_j^i; \theta^i) + \epsilon_j^i,$$

128 where $\epsilon_j^i \sim \mathcal{N}(0, \sigma_j^i)$ is the gaussian-distributed error model. The latter was either constant ($\sigma_j^i =$
129 $a, \forall i, j$) for TK or proportional ($\sigma_j^i = bM(t; \theta), \forall i, j$) for BK. To describe inter-individual variability,

It is made available under a [CC-BY-NC-ND 4.0 International license](https://creativecommons.org/licenses/by-nc-nd/4.0/) .

130 individual parameters θ^i were assumed to follow log-normal distributions:

$$\ln(\theta^i) = \ln(\theta_{\text{pop}}) + \eta^i, \quad \eta^i \sim \mathcal{N}(0, \omega^2)$$

131 with population-level parameters θ_{pop} and ω . Estimation of these was performed using the stochastic approximation of expectation maximization algorithm implemented in the Monolix software^{30,31}.

133 Structural models

134 Following previous work, the TK structural model was assumed to be the sum of two exponentials^{19,32}:

$$y_j^i = \begin{cases} y_0^i e^{KG^i t} & t \leq 0 \\ y_0^i (e^{-KS^i t} + e^{KG^i t} - 1) & t > 0 \end{cases}$$

136 where $t = 0$ corresponds to treatment initiation and y_0 , KG and KS are three parameters. This model was also considered for BK, together with three other models: constant ($y_j^i = \alpha^i, \forall j$), linear ($y_j^i = \alpha^i + \beta^i t_j^i, \forall j$) and hyperbolic ($y_j^i = p^i + \frac{e^{i^i}(q^i - p^i)}{t_j^i + e^{i^i}}$). Quantitative comparison of goodness-of-fit between models was assessed using the corrected Bayesian information criterion³³.

140 Identification of individual model-based parameters

141 The population parameters identified on the training set were used to define prior distributions of the TK and BK model parameters. These “training” priors were used for Bayesian estimation (maximum a posteriori estimate) of the individual TK and BK model parameters, in both the training and testing sets. To avoid biased comparison with baseline variables, the model-estimated baseline parameters (y_X^0 for $X = \text{TK, CRP, LDH}$ and neutrophils, and albumin_q for albumin) were not kept in the TK and BKs feature sets. We additionally considered the ratio of the model-predicted value at cycle 3 day 1 to the model-estimated baseline parameter, denoted X_{ratio} for marker X . Altogether, there were three individual parameters for each marker: X_{KG} , X_{KS} and X_{ratio} for $X = \text{TK, CRP, LDH}$ and neutrophils; and albumin_p, albumin_l and albumin_{ratio} for albumin. Once centered and scaled (from means and standard deviations derived from the training set), these individual model-based parameters constituted the TK and BKs feature sets.

152 Truncated data: individual-level

153 Individual-level truncated datasets were derived from the longitudinal TK and BK data at the following treatment cycle horizons: cycle 3 day 1 (C3D1, 1.5 months), C5D1 (3 months) and C10D1 (6.75 months). That is, for each patient, post-CXD1 values were discarded, for both the training and testing sets. New training priors were estimated from each CXD1 training set and used for Bayesian estimation of the individual parameters in the CXD1 training and testing sets. The resulting TK and BK truncated model parameter Y for marker X at cycle horizon i were denoted by $X_{Y,i}$ (e.g., $ldh_{KG,5}$).

159 Truncated data: study-level

160 To assess the ability of kML to early predict the final outcome of a clinical trial, we considered the two arms of the OAK phase 3 study. That is, not only the atezolizumab arm (testing set) but also the docetaxel arm (unused previously). For each arm, the data was truncated at multiple on-study landmark times l_t ($l_t = 10, 25$ and 60 weeks) after study initiation (first patient recruited). That is, only the patients enrolled before this time and only the data collected up to l_t was used. For both arms the NLME population priors estimated from the training set (atezolizumab monotherapy) was used for Bayesian estimation of the individual model parameters, for each on-study-truncated dataset. For example, for a patient i recruited at 12 weeks, it was absent from the $l_t = 10$ weeks data set, had model parameter values $\theta_{l_t=25}^i$ derived from 13 weeks of on-study data in the $l_t = 25$ weeks data set and different model parameter values $\theta_{l_t=60}^i$ derived from 48 weeks of on-study data in the $l_t = 60$ data weeks set.

171 Machine learning

172 Models

173 Model elaboration and development was performed exclusively on the training set, using 10 folds
174 cross-validation for predictive performances evaluation. Due to censoring in the data, survival
175 models were used: proportional hazards Cox regression³⁴, extreme gradient boosting (XGB) with
176 either Cox or accelerated failure time (AFT) models³⁵ and random survival forests²³. Nested cross-
177 validation with inner bagging in each 10-fold cross-validation outer loop was used to evaluate the
178 benefit of tuning the hyperparameters³⁶. Improvement of the performances was negligible with
179 hyperparameter tuning, that has higher computational cost (Appendix 1—figure 15). Therefore,
180 we used the default values of the hyperparameters (that is, number of trees $n_{tree} = 500$, number
181 of variables to possibly split at each node $m_{try} = 5$ (rounded up square root of the number of
182 variables), minimum size of terminal node $n_{odesize} = 15$, non-negative integer specifying number
183 of random splits for splitting a variable $n_{split} = 10$ for the RSF model).

184 Evaluation

185 Predictive performances were assessed for either discrimination (c-index and classification met-
186 rics at horizon times τ), calibration (calibration curves) or stratification (dichotomized KM survival
187 curves). For each individual, the RSF model gives two prediction outputs: a scalar value termed
188 “mortality” that we will refer to as “ML score”, and time-dependent predicted survival curves²³. The
189 former was used to compute the c-index using the `rcorr.cens` function of the `hmisc` R package^{37,38}.

190 For classification (prediction of survival at a horizon time τ), we used the latter to compute
191 model-predicted probabilities of death at τ . Unless otherwise specified, $\tau = 12$ months. Survival-
192 adapted metrics of predictive performance were used for sensitivity, specificity, area under the
193 receiver-operator curve (ROC AUC) and negative and positive predictive value (NPV and PPV) to ac-
194 count for censoring^{39,40}. For computation of accuracy, censored patients before τ were discarded
195 ($N = 17/396$ in the test set at 12 months). Event was defined as death. Therefore, e.g., PPV cor-
196 responds to the ability of the model to correctly predict death. The optimal cut-points used for
197 individual OS predictions on the test set were defined as the Kaplan-Meier estimated OS in the
198 training set at τ (0.257 at 6 months, 0.437 at 12 months, 0.634 at 24 months).

199 For patient stratification (dichotomized KM curves), the ML score was used, with models trained
200 on the training set and predicted on the test set. In order to assess stratification abilities to capture
201 the 20% of long-term survivors, cut-points were set at the 20th percentiles for each variable/score
202 evaluated. For fair comparisons, the population was also restricted to the patients with enough
203 data to be predicted by the ML model (see preprocessing above). Significance of differences in KM
204 curves was established using the logrank test, and hazard ratios were computed using proportional
205 hazards Cox regression.

206 Variable selection and minimal signature

207 Three strategies were investigated to account for the multi-modal nature of the data: 1) variable
208 selection on all the variables together, 2) variable selection per feature set (clinical, RNAseq, TK
209 and BK) or 3) variable selection on the pooled sets resulting from 2). The general method for
210 variable selection in a feature set was based on two steps: i) sorting the variables by importance
211 and ii) building incremental models including increasing numbers of variables. For i), multiple al-
212 gorithms were tested: Cox-sorting based on either univariate p-values or absolute hazard ratios,
213 backward/forward stepwise selection, variable importance from RSF, or least absolute shrinkage
214 and selection operator (LASSO)-based importance⁴¹. The latter was the one ultimately selected.
215 It was defined as the sorting resulting from coefficients gradually becoming non-zero during like-
216 lihood maximization, when the regularization parameter λ decreases. For ii), the algorithm used
217 for incremental models was RSF. Resulting c-indices and AUCs were plotted against the number
218 of variables. Selected variables were defined as the minimal subset of variables able to reach the
219 maximum c-index. Minimal signatures were defined as the minimal set of variables able to achieve

Table 1. Parameters from nonlinear mixed-effects modeling of tumor and blood marker kinetics

	K		CRP		LDH		Neutrophils		Albumin		
KG_{pop} (week ⁻¹)	0.00492	(6.80)	0.00814	(9.38)	0.00238	(10.48)	0.00436	(8.69)	p_{pop} (g/l)	29.4	(3.82)
KG_{pop} (week ⁻¹)	0.00778	(8.22)	0.0137	(14.14)	0.00184	(13.73)	0.000987	(21.16)	l_{pop} (log (day))	8.09	(2.74)
ω_{KG}	1.36	(3.80)	1.61	(4.25)	1.55	(5.36)	1.41	(4.48)	ω_p	0.476	(7.48)
ω_{KS}	1.41	(4.66)	1.81	(6.29)	1.92	(5.34)	2.46	(5.82)	ω_l	0.359	(6.42)
error ¹	6.82	(1.15)	0.559	(1.23)	0.138	(0.79)	0.207	(0.82)	error ¹	0.0549	(0.77)

Parameter value (relative standard error (%)). TK: constant error, others: proportional error. CRP : C-reactive protein; LDH : lactate dehydrogenase.

220 a c-index larger than 0.75 and an AUC larger than 0.8.

221 Survival simulations and computation of predicted HRs

222 For each patient i , one output of the kML model is a survival curve $S^i(t)$. This gives the cumulative
 223 distribution function $1 - S^i(t)$ of the random variable T^i of the time to death for patient i , which
 224 was used to simulate 100 replicates of T^i . Pooling all patients together, we thus obtained 100 repli-
 225 cates of $\{T^{i,ATZ}, T^{j,DTX}\}$ for i and j being the patient indices within the ATZ and docetaxel arms,
 226 respectively. Each replicate then led to 1) a predicted survival curve in each arm and 2) a Cox pro-
 227 portional hazard HR between the two arms. Taking the mean and the 5th and 95th percentiles over
 228 all replicates yielded the reported point estimate and corresponding 95% prediction interval. The
 229 same procedure was used for study-truncated data.

230 Results

231 data

232 The data consisted of individual measurements of NSCLC patients treated with ATZ monotherapy.
 233 Three phase 2 trials were pooled into a training dataset^{3,25,26} ($N = 862$ patients, Appendix 1—figure
 234 1). The external validation (test) set comprised data from the OAK phase 3 trial ($N = 553$)²⁷.

235 Variables comprised baseline (pre-treatment) and longitudinal (on-treatment) data (Figure 1A).
 236 The former included: patients and disease characteristics ($p = 63$ variables, 43 numeric and 20
 237 categorical, denoted BSL) and transcriptomic (“RNAseq”, $p = 58,311$ transcripts) data. The latter
 238 included: longitudinal investigator-assessed sum of largest diameters (SLD) of lesions as per the
 239 RECIST criteria⁴², denoted by tumor kinetics (TK, $k = 5, 473/3, 015$ time points in the train/test sets, re-
 240 spectively, median 5/4 data points per patient, range 2/2 —24/20); and longitudinal measurements
 241 of four blood markers (albumin, C-reactive protein (CRP), lactate dehydrogenase (LDH) and neu-
 242 trophils), denoted together as blood markers kinetics (BK, $k = 60, 779/38, 460$ data points, median
 243 11–7–11–11/9–9–9–10 data points per patient, range 3–3–3–3/3–3–3 —60–63–63–78/82–47–77–89 for
 244 albumin–CRP–LDH–neutrophils in the train/test sets, respectively). See Figure 1B and Appendix
 245 1—figure 2–4 for details of the data and overall algorithmic procedures.

246 Nonlinear mixed-effects modeling (NLME) of longitudinal markers

247 The TK structural model was the sum of an increasing and a decreasing exponential function (dou-
 248 ble exponential model)³². It was able to accurately describe the data with no goodness-of-fit mis-
 249 specification (Figure 2A and Appendix 1—figure 5). Population parameters were estimated with
 250 good accuracy (all relative standard errors smaller than 9%, Table 1).

251 To analyze the BK data, we first investigated whether significant kinetic patterns could be ob-
 252 served beyond random noise (due to, e.g., measurement errors, see raw data in Appendix 1—
 253 figure 6–9). The latter was considered as the null hypothesis, described by a constant model. It
 254 was tested against three alternative empiric models: linear, hyperbolic (monotonous but nonlin-
 255 ear and saturating) and double-exponential (nonlinear and non-monotonous). For all four BKs,
 256 we found significant kinetics compared with the constant model, as shown by lower corrected

Figure 1: Study schematic

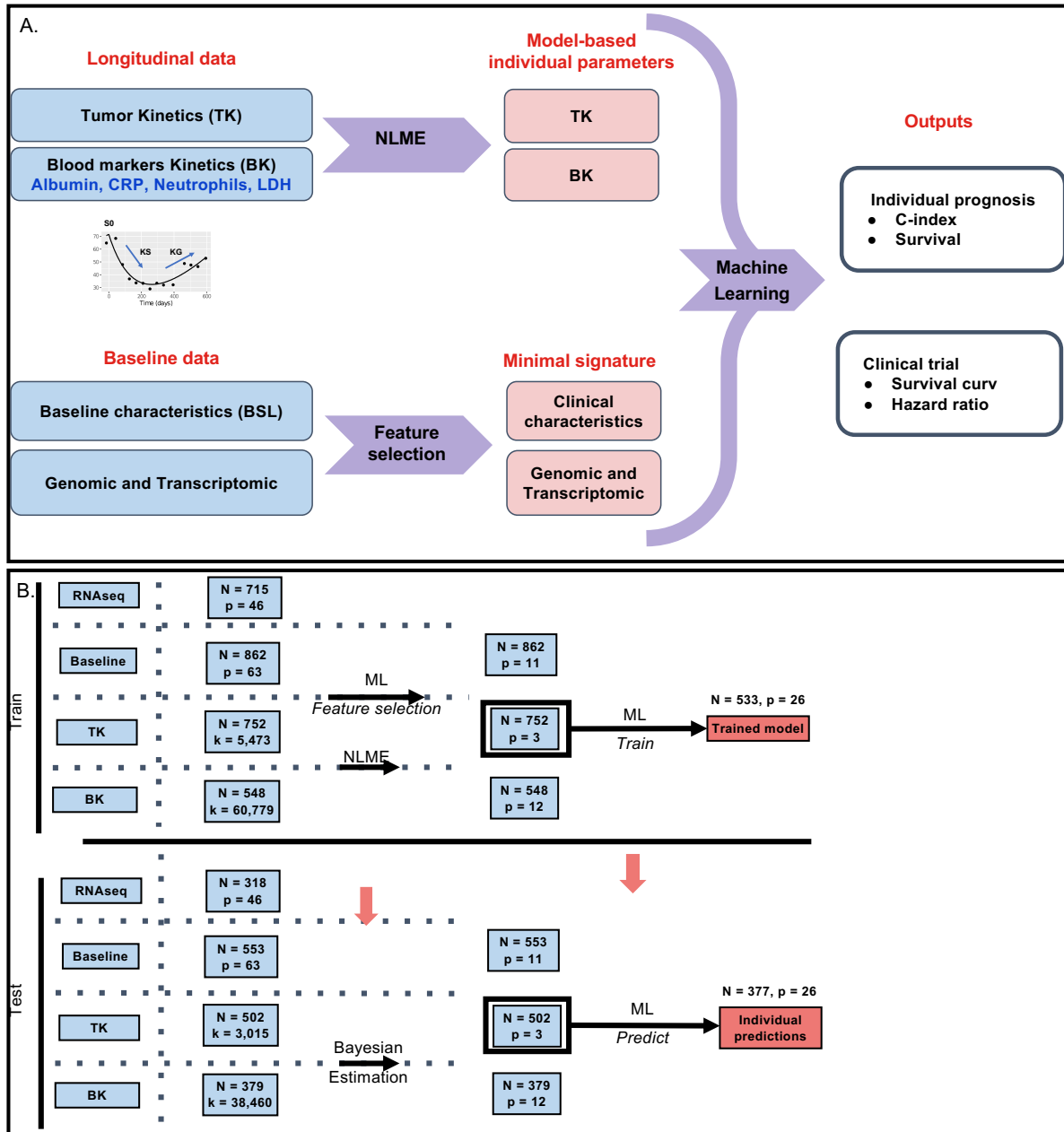


Figure 1. Study schematic **A.** Baseline and longitudinal data were combined into a machine learning algorithm in order to predict individual survival prognosis. Longitudinal data were modelled using nonlinear mixed-effects modelling, whereas machine learning-based feature selection was applied to the baseline data to derive a minimal signature. Tumor kinetics and biological kinetics parameters were combined with the minimal signature to predict survival. Predictive performances were assessed using survival metrics (c-index and survival at horizon times).

B. Algorithm used to develop the model on the train data and carry it to the test set for external validation. Each step — preprocess, learning of the Bayesian priors, dimensionality reduction, feature selection, choice, tuning and training of the machine learning algorithm — were calibrated on the training set and then applied to the test set.

TK: tumor kinetics; BK: blood markers kinetics; ML: machine learning; NLME: nonlinear mixed-effects modelling

Figure 2: Goodness-of-fit metrics and plots of dynamic BK models

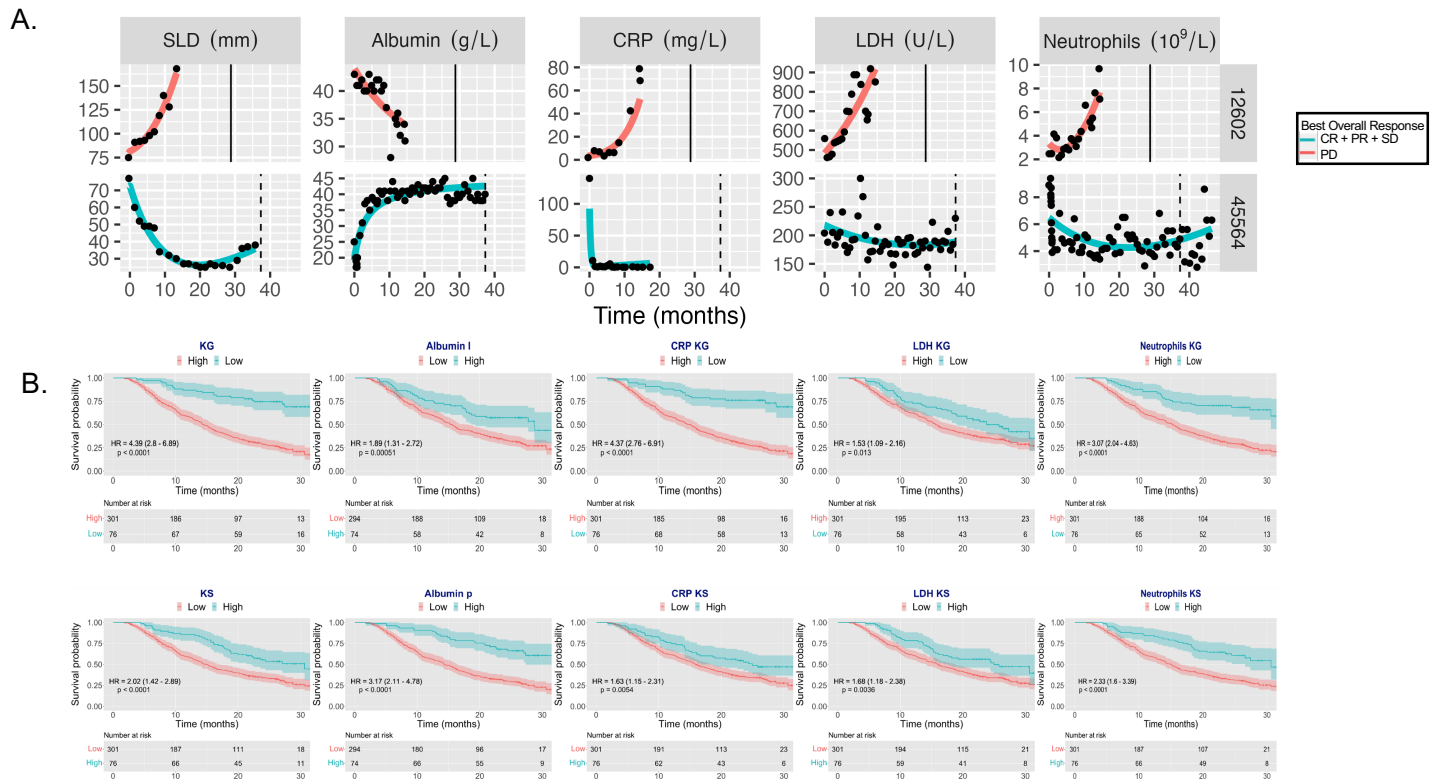


Figure 2. Goodness-of-fit metrics and plots of dynamic BK models **A.** Representative individual fits for the TK and BK best empirical models showing non-trivial kinetic parameters well captured by the dynamic models. Survival is indicated by a vertical line (solid = death, dashed = censored). **B.** Stratified Kaplan-Meier curves at the 20th percentile level on the test set, for TK and BK model-based parameters. Missing values were removed in this univariable analysis, explaining the difference of initial number of patients for albumin that had 9 patients in this case. CR: complete response; PR: partial response; SD: stable disease; PD: progressive disease.

257 Bayesian information criterion and relative error between model fits and data (Appendix 1—figure
 258 10). Best descriptive models were hyperbolic for albumin and double-exponential for the other
 259 BKs. Individual fits to patient kinetics with the best models showed substantial descriptive power
 260 (Figure 2A), which was confirmed by data versus model fits plots (11–14). Parametric identifiability
 261 of population parameters was excellent for all models (Table 1).

262 We further assessed the stratification value of the individual model-based kinetic marker for
 263 OS prognosis (Figure 2B). The TK parameter KG (growth rate) exhibited good stratifying ability
 264 ($HR = 4.39 (2.8 - 6.89)$), which was similar to the CRP_{KG} parameter ($HR = 4.37 (2.76 - 6.91)$). Ranked
 265 by HR importance, the following four best parameters were $albumin_p$ ($HR = 3.17 (2.11 - 4.78)$),
 266 $neutrophils_{KG}$ ($HR = 3.07 (2.04 - 4.63)$), $neutrophils_{KS}$ ($HR = 2.33 (1.6 - 3.39)$) and TK_{KS} ($HR = 2.02$
 267 $(1.42 - 2.89)$). All kinetic parameters carried substantial prognostic power ($p < 0.0001$, log rank test).

268 For TK and BKs we complemented the initial model parameters with an additional metric that
 269 was considered valuable for early prediction: the model-predicted ratio of change over baseline at
 270 cycle 3 day 1.

271 Overall survival prediction using kinetics-machine learning (kML): 272 model development

273 Four feature sets resulted from the analysis above: BSL, RNAseq, TK and BK (Figure 1B). The devel-
 274 opment of a kinetics-machine learning (kML) comprised two main steps: choice of the algorithm

It is made available under a [CC-BY-NC-ND 4.0 International license](https://creativecommons.org/licenses/by-nc-nd/4.0/).

275 and derivation of a minimal signature. They were performed using cross-validation on the training
276 set. The first was achieved by benchmarking four models that used all variables ($p = 119$, $N = 553$).
277 The random survival forest (RSF) model was selected as it exhibited the best performances (Ap-
278 pendix 1—figure 15). Notably, we found significantly better predictive performances of RSF over a
279 Cox proportional hazard regression model ($p = 0.0006$).

280 Feature selection on BSL variables was performed building incremental RSF models based on
281 LASSO importance-sorted variables (Figure 3A). The model using all of them achieved the best
282 score. Nevertheless, keeping in mind the objective to ultimately support decision making and pa-
283 tient stratification, a minimal (11 features), near-optimal, set of BSL variables was selected and
284 denoted mBSL. It was defined as the first seven variables reaching the plateau (CRP, heart rate, neu-
285 trophils to lymphocytes ratio, neutrophils, lymphocytes to leukocytes ratio, liver metastases and
286 ECOG score), complemented with four variables with established prognostic or predictive value
287 and available in routine care: PD-L1 expression (50% cut-off)³, hemoglobin⁴³, SLD²² and LDH^{44,45}.

288 Applying stringent criteria to the RNAseq data (see methods), we selected 167 transcripts as
289 candidates for final variable selection using Bolasso regression model to identify the optimal set
290 of predictors²⁸. Finally, we ended up with 52 RNAseq variables that corresponded to the highest
291 average c-index of 0.64.

292 Performing incremental models with BKs, the first four LASSO-based most important features
293 were LDH_{KG}, neutrophils_{KG}, albumin_p and CRP_{KG} parameters were the four most important fea-
294 tures (not shown). This indicated that the combination of all BKs was required to achieve signifi-
295 cant predictive performances. Nevertheless, we kept all sets of three model-based parameters in
296 the TK and BK signatures (15 parameters in total) because each set depends only on one marker
297 (per time point).

298 We then compared the cross-validated c-index of each feature set on the train data (Figure
299 3B). Because of negligible discrimination performances ($c\text{-index} = 0.62 \pm 0.050$) and non-systematic
300 availability of those data, the RNAseq set was removed from the model. The selected set of clinical
301 data at baseline (mBSL) exhibited moderate discrimination performances ($c\text{-index} = 0.710 \pm 0.038$),
302 which was slightly outperformed by the TK set ($c\text{-index} = 0.723 \pm 0.025$). Interestingly, the BK set
303 significantly outperformed both baseline clinical and TK ($c\text{-index} = 0.793 \pm 0.038$, $p = 0.0004$ and 0.0005
304 respectively, Student's t-test). Jointly, mBSL, TK and BK performed significantly better than any
305 feature set alone ($c\text{-index} = 0.824 \pm 0.050$, $p = 0.00007$, 0.0002 and 0.055), as well as any combination
306 of two sets among the three (mBSL + TK: $c\text{-index} = 0.77 \pm 0.026$, mBSL + BK: $c\text{-index} = 0.81 \pm 0.027$,
307 TK + BK: $c\text{-index} = 0.80 \pm 0.049$). The resulting model combining mBSL, TK and BK was denoted kML
308 (kinetics-machine learning).

309 During cross-validation on the training set, kML exhibited excellent predictive performances
310 across multiple metrics, with minimal between-folds variability ($AUC = 0.919 \pm 0.056$, $accuracy =$
311 0.873 ± 0.052 , Figure 3C).

312 External validation

313 The predictive performance of the final kML model (mBSL, TK and BK) was assessed on the test
314 set (377 patients). At the population level, the model-predicted survival curve was in excellent
315 agreement with the observed data (Figure 4A). Notably, the prediction interval from the model
316 was narrow, indicating high precision. At the individual level, consistent with the cross-validation
317 results, substantial discrimination performances were observed ($c\text{-index} = 0.789$, Figure 4B, AUC
318 for 12-months survival probability = 0.874). All classification metrics for prediction of survival at 12
319 months were high (≥ 0.78), except PPV. Although smaller, they were similar to the cross-validation
320 results.

321 In addition, calibration curves revealed good performance, at multiple horizon times (Figure
322 4C). Model-predicted probabilities were concordant with the observed KM estimates of the survival
323 probabilities, over the entire range of the binned predicted probabilities. This is further illustrated
324 by the contingency Table 2. For instance, among 149 patients predicted to be dead at 12 months,

Figure 3: Minimal baseline (mBSL) signature and kinetics-ML (kML) model

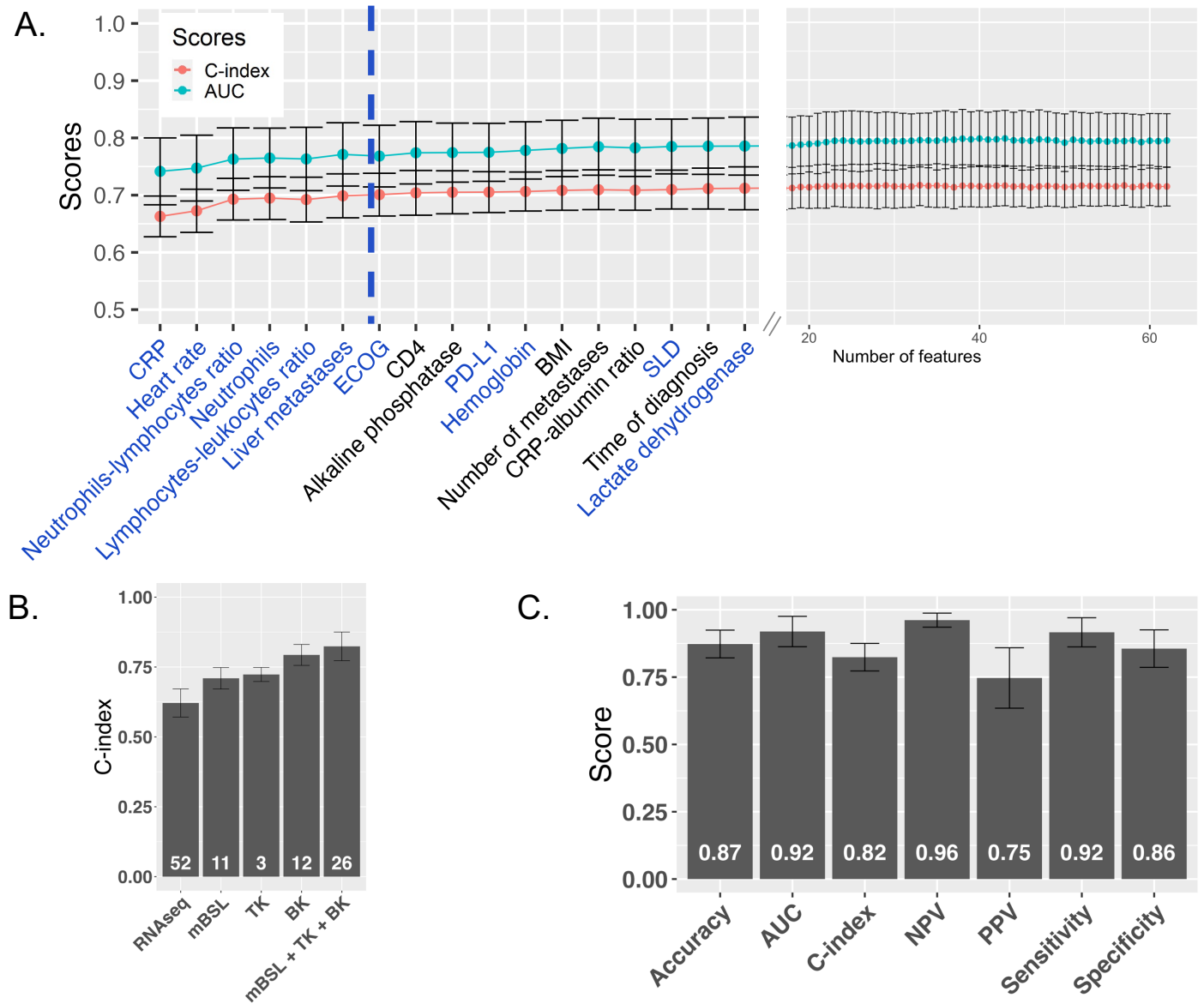


Figure 3. Minimal baseline (mBSL) signature and kinetics-ML (kML) model **A.** Cross-validated (CV) performance scores on the training set (c-index and AUC, mean \pm standard deviation) for incremental random survival forest (RSF) models using an increasing number of baseline clinical and biological variables sorted by LASSO importance. The dashed blue line shows the minimal number of variables reaching the plateau. Blue-colored variables correspond to the minimal clinical signature (mBSL). **B.** Comparative CV c-indices of RSF models based either on RNAseq, mBSL, TK, BK and mBSL + TK + BK (final model, kML) variables showing increased predictive performances over baseline when using model-based parameters of kinetic markers. Numbers on the bars indicate the number of variables. **C.** CV performances of the kML model for discrimination (c-index) and classification (survival prediction at 12-months OS).

Table 2. Contingency table for OS prediction at 12 months

MODEL		TRUTH		
		Alive (0)	dead (1)	Total
	Alive (-)	182	30	212 (58.7%)
	Dead (+)	48	101	149 (41.3%)
	Total	230 (63.7%)	131 (36.3%)	361

Note: 16/377 censored patients with survival time ≤ 12 months removed for computation of accuracy. sensitivity, specificity, PPV and NPV don't correspond exactly to the numbers because they are computed from KM estimate, thus adjusting for censoring bias.

101 (67.8%) were actually deceased. Predictive AUC was good at other horizon times (0.846 and 0.910 at 6 and 24 months, respectively, Appendix 1—figure 16). However, PPV and sensitivity were very low at 6 months.

Notably, the kML mortality score derived from the model and learned on the training set was able to accurately stratify OS in the test set (HR = 25.2 (10.4–61.3), $p < 0.0001$, Figure 4D), indicating excellent ability to identify the 20% of long-term survivors. It outperformed all single kinetic markers (Figure 2C).

Variables importance was assessed by running a post-hoc multivariable Cox regression (Figure 4F). Interestingly, the top two variables were BKs (CRP_{KG} and CRP ratio C3). In addition, TK and BK made up for six out of the seven top important features and were found more important than PD-L1.

Given the large sample size of our data, we further assessed the model performances when trained on smaller data sets (Appendix 1—figure 17). The learning curve revealed that approximately 200 patients were necessary to reach similar performance to the ones obtained with the full training set ($N = 533$), for both cross-validation and external validation on the test set ($c\text{-index} = 0.82 \pm 0.056$ vs $c\text{-index} = 0.82 \pm 0.050$ in cross-validation, 0.78 vs 0.79 on the test set, models trained with 200 vs 533 patients, respectively). Trained with only 60 patients, kML reached already good performances ($c\text{-index} = 0.76 \pm 0.15$ and 0.74 in cross-validation and test, respectively).

Together, these results demonstrate important predictive performances of overall survival following ATZ treatment using the kML model.

Application to individual survival prognosis from early on-treatment data

Results above required full on-treatment time-course data to compute TK and BK markers, thus cannot be used to make early predictions of future survival. To investigate the operational applicability of our methodology, data from the test set were truncated at the beginning of treatment cycles number three, five or ten, respectively corresponding to 1.5, 3 and 6.75 months. We found that integrating longer on-treatment data in kML, the predictive performances steadily increased (Figure 5A and Appendix 1—figure 18). Using the baseline variables only (mBSL), the stratification ability was significant but moderate (HR = 1.74 (1.24–2.46), $p = 0.0014$, Figure 5B). In contrast, kML exhibited increasing stratification ability from data at 1.5 months (HR = 2.19 (1.53–3.12), $p < 0.0001$), 3 months (HR = 3.51 (2.33–5.3), $p < 0.0001$) and 6.8 months (HR = 5.01 (3.16–7.95), $p < 0.0001$), see Figure 5C.

Further investigation of the predictive performances of individual kinetic markers revealed that TK parameters were the most informative at 6 weeks (1.5 months, first imaging assessment). Adding BKs to TKs brought additional predictive value starting at 3 months, and BKs outperformed TK from 6.75 months on (Appendix 1—figure 19A). Among BKs, neutrophils kinetics appeared to be the most predictive, followed by CRP, albumin and LDH. However, the combined BK signature outperformed each individual BK, indicating that their collective predictive capabilities were not

Figure 4: Predictive performances on the test set

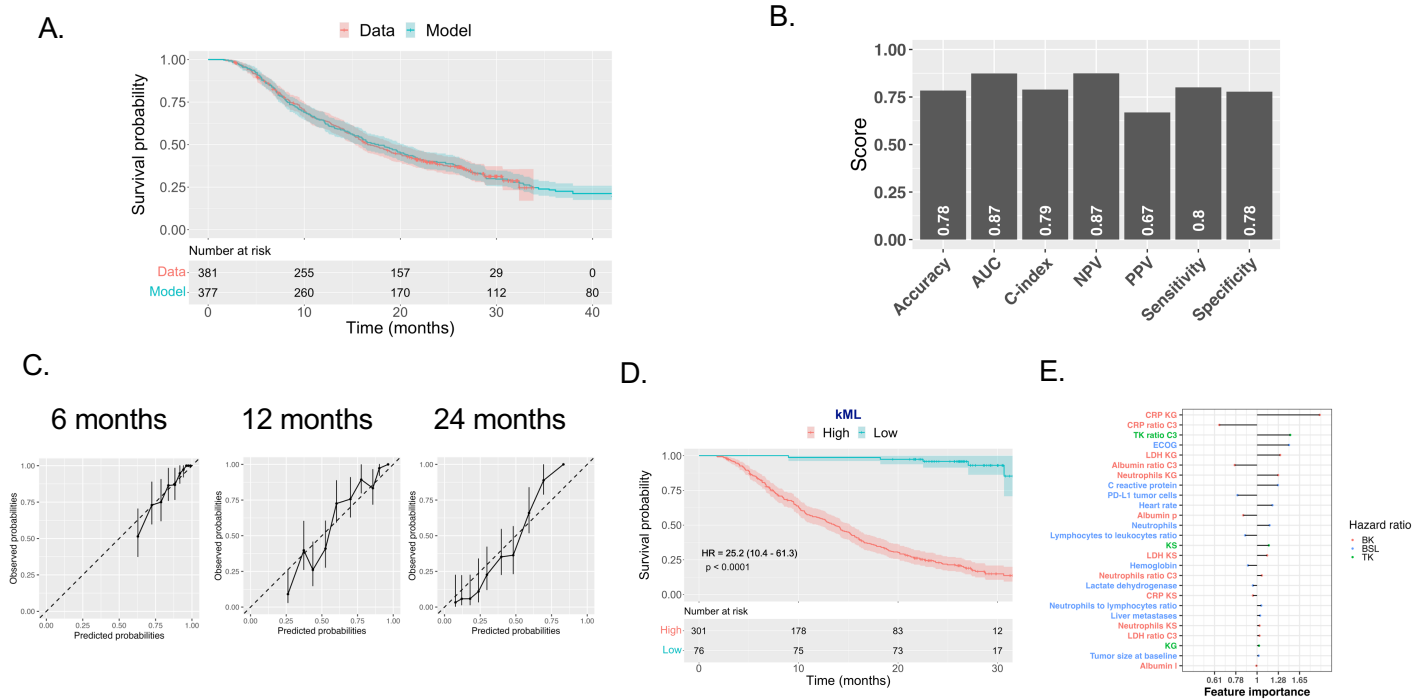


Figure 5: Individual-level predictions from cycle-truncated data

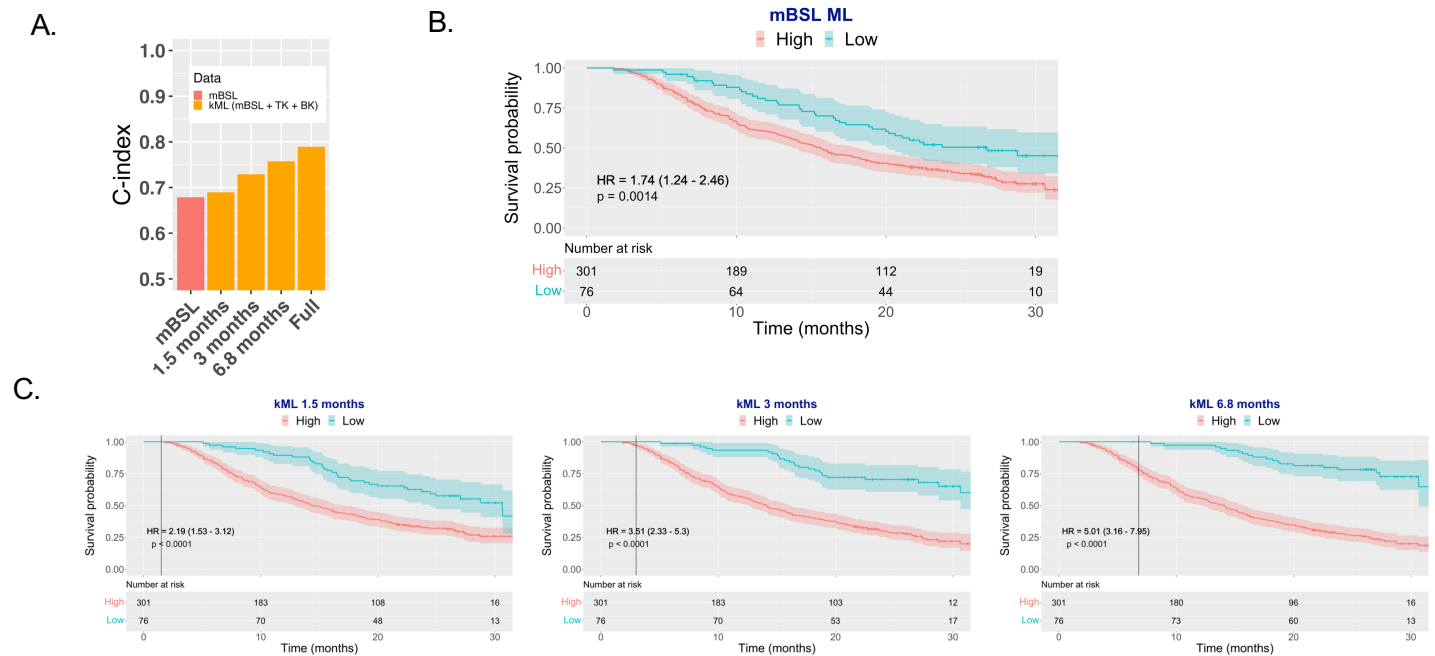


Figure 5. Predictive value from cycle-truncated data **A.** Predictive power (c-index) of ML models using baseline (BSL) or truncated data at 1.5, 3 and 6.8 months as well as the full time-course. **B.** Stratified KM survival curves using a RSF model trained on the minimal baseline (mBSL) variables. **C.** Stratified KM survival curves using kML from 1.5 months (2 cycles), 3 months (4 cycles) and 6.8 months (9 cycles) truncated data. Truncation time is indicated by the vertical line.

TK: tumor kinetics; BK: biological kinetics; LDH: lactate dehydrogenase; CRP: C-reactive protein.

362 driven by any single biomarker alone.

363 Interestingly, the most important variable at 1.5 months was a kinetic one, TK ratio C3 with
 364 following variables being from mBSL (e.g., liver metastases, PDL1 and ECOG). When more on-
 365 treatment variables become available, this shifted to TK and BK (TK ratio C3, TK_{KS}, TK_{KG}, CRP_{KG},
 366 LDH_{KG}), see Appendix 1—figure 19B.

367 Application to clinical trial outcome prediction from early on-study data

368 The kML model can also be applied for the prediction of the outcome of a clinical trial (survival
 369 curves and associated hazard ratio), from early on-study data. To this respect, a different trun-
 370 cation needs to be performed. Indeed, the quantity of data available is not determined by the time
 371 a given patient has received the treatment, but rather by the recruitment rate and the number
 372 of patients and associated data available at a given on-study landmark time. We thus performed
 373 such truncations on the test set based on a number of weeks after the date of the first patient
 374 recruited. Predictions of the kML model applied to each arm (atezolizumab and docetaxel) yielded
 375 very accurate results when using data from the entire study (predicted HR = 0.784 (0.7–0.842)),
 376 versus data HR = 0.778 (0.65–0.931), Figure 6A–B). Notably, the model prediction intervals were
 377 narrower than the data Kaplan-Meier confidence intervals. Using only early data, the model was
 378 already able to detect a (non-significant) tendency at 10 weeks, with only 23 and 30 patients in each
 379 arm, and very small follow-up. Starting from data available at 25 weeks (6.25 months), the model
 380 correctly predicted a positive outcome of the study, with a 95% prediction interval of the HR below
 381 1. Of note, the available data at this time (dashed lines, Figure 6A and red HR CIs in Figure 6B) was
 382 far from being conclusive. The model prediction was stable from 25 weeks on whereas the data
 383 only exhibited significant HR from 60 weeks and required more than 300 patients in each arm to

384 be conclusive.

385 Discussion

386 Blood markers from hematology and biochemistry are routinely collected during clinical care or
387 drug trials. They are cost-effective and easily obtained both before and during treatment. There
388 is limited exploration regarding the predictive capabilities of the kinetics of such data. Combining
389 BSL variables with on-treatment data (TK and BK), we addressed this question using a novel hy-
390 brid NLME-ML methodology. The resulted kML model demonstrated excellent predictive perfor-
391 mances for OS in two aspects: 1) patient-level predictions (discrimination, calibration and patient
392 stratification) and 2) trial-level predictions. The kML model outperformed current state-of-the-art
393 methods based on either baseline or on-treatment data alone, utilizing only routine clinical infor-
394 mation, with a c-index of 0.79 and an area under the curve (AUC) of 0.87 on the test dataset. Overall,
395 kML incorporates 26 features, out of which 15 features require monitoring five quantities over time
396 (tumor size, albumin, CRP, LDH and neutrophils).

397 Regarding baseline markers, the predictive value of PD-L1 expression, commonly used in clini-
398 cal care, is controversial^{9,10}. Previous studies reported an AUC for durable response of 0.601 and
399 a PFS HR of 1.90 (PD-L1 \geq 1% vs 0%)⁸. Baseline tumor mutational burden showed similar predictive
400 value initially (AUC = 0.646)¹¹, but led to disappointing results in a recent prospective study⁴⁶ and
401 others found it to be more prognostic than predictive⁴⁷. Baseline blood counts were previously
402 reported to predict overall survival^{44,48-50} and treatment response (AUC = 0.74)⁴³. The ROPRO
403 score, derived from a large pan-cancer cohort and incorporating baseline clinical and biological
404 data (27 variables) achieved a c-index of 0.69 and a 3-months AUC of 0.743 for prediction of survival
405 in the OAK clinical trial⁵¹. Here, we confirmed these findings and established a minimal signature
406 of such data composed of only 11 variables (CRP, heart rate, neutrophils to lymphocytes ratio, neu-
407 trophils, lymphocytes to leukocytes ratio, liver metastases, ECOG, PD-L1 \geq 50%, hemoglobin, SLD
408 and LDH), yet with similar predictive performances (*c-index* = 0.678) and significant stratification
409 ability (HR = 1.74, p = 0.0014). Altogether, our kML model demonstrated substantially better predic-
410 tive performances than these baseline models.

411 The main novelty of our work lies in the use of on-treatment blood markers kinetics (BK). We
412 first further confirmed the established predictive value of TK model-based parameters^{19,20}. Blood-
413 or serum-derived longitudinal markers kinetics have to date rarely been modeled. Gavrilov et al.
414 proposed to model NLR kinetics and demonstrated improved OS predictions over TK alone⁵². Here
415 we extended to four BKs: albumin, CRP, LDH and neutrophils. This choice was not only motivated
416 by observed statistical associations, but also from biological considerations. Albumin is associated
417 with nutritional status (cachexic state) and is known to evolve with time in responders. CRP is a
418 marker of systemic inflammation⁴⁵. Increased CRP, decreased albumin level, and increased CR-
419 P/albumin ratio have been reported to be associated with poor survival⁵³. Neutrophils play a role
420 in inflammation by promoting a favorable microenvironment for cancer cell growth and spread,
421 and activation of carcinogenic signaling pathways⁵⁴. Elevated LDH levels are a marker of cancer
422 cells turnover rate, and LDH has a potential role for prediction of potential invisible metastases⁴⁵.
423 We found that all these markers had non-trivial on-treatment kinetics. However, data fits were not
424 perfect, possibly due to the simplicity and empiric nature of the models we used. Further mecha-
425 nistic modeling of the joint kinetics of BKs and TK could bring relevant biological information and
426 yield more accurate predictive parameters. We found that all four BKs were contributive to the
427 model and that, combined, they outperformed TK performances.

428 We analyzed the RNAseq data using standard methods and found only negligible predictive
429 performances. Such result could be explained by the fact that the tissue of origin that was used
430 was heterogeneous across the patients (primary tumor or metastasis), was limited to a local area
431 of the tumor, and could come from tissue sampled long before treatment initiation. Given that
432 our main objective was to derive a predictive model from markers available in routine practice, we

Figure 6: Use of kML for early prediction of the outcome of a clinical trial

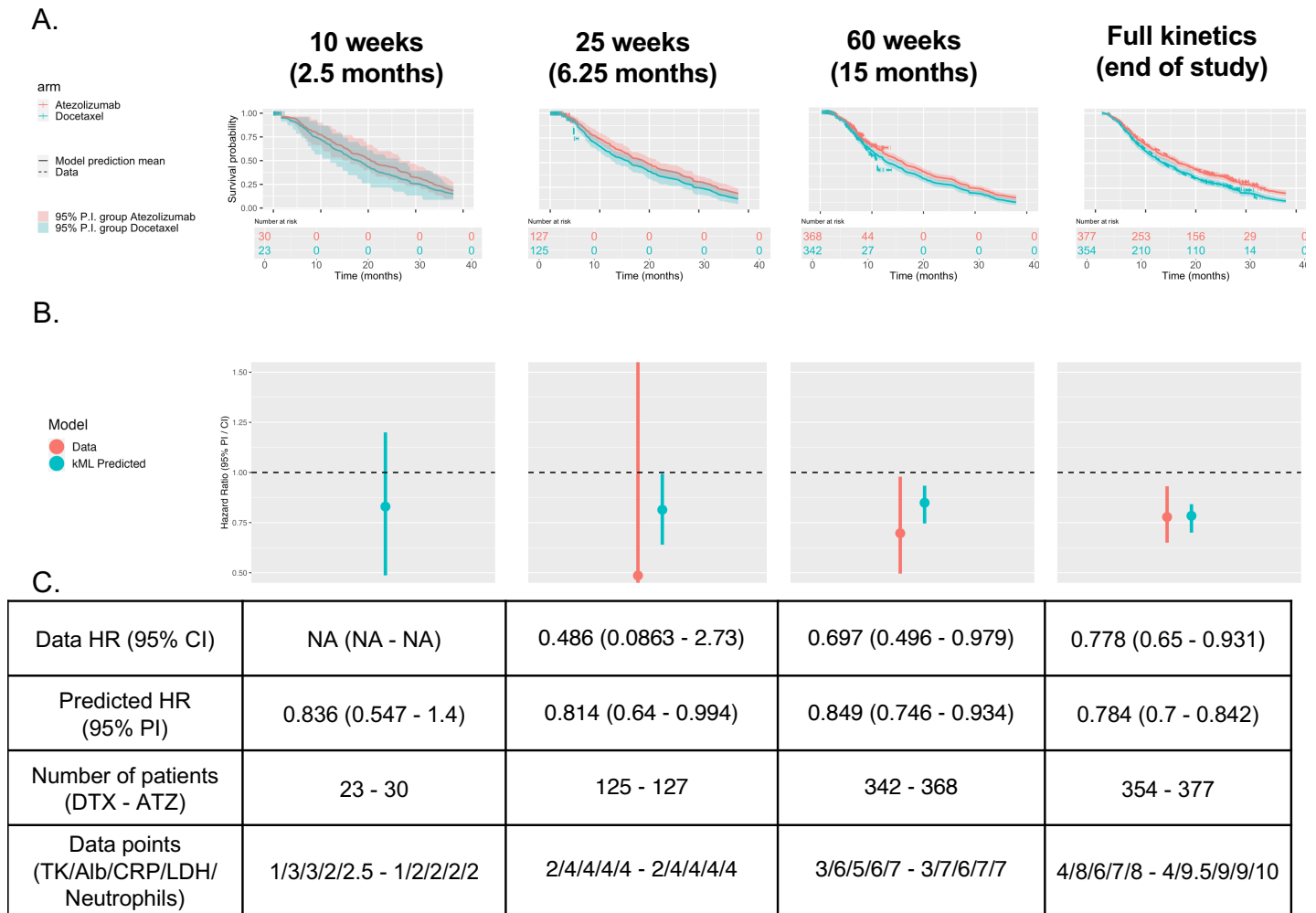


Figure 6. Use of kML for early-prediction of the outcome of a clinical trial **A.** Survival curves model-based predictions and prediction intervals versus actual data from on-study data at multiple horizon times after study initiation. Note that the model is able to predict full survival curves even if based on early kinetics. **B.** Compared data and kML-predicted hazard ratios. **C.** Description of hazard ratios, number of patients and number of data points available in each arm, at the landmark on-study time points. PI: prediction interval, CI: confidence interval, DTX: docetaxel arm, ATZ: atezolizumab arm.

433 excluded it from our minimal signature. A refined analysis, especially focusing on immune-based
434 signatures, could improve our results⁵.

435 Machine learning models, although increasingly used in pharmacological studies —including
436 recently for TK-OS modeling and variable selection^{22,55} —have yet rarely been rigorously compared
437 to classical statistical models²⁴. Here, such comparison revealed significantly better performance
438 of the nonlinear random survival forest RSF model compared to the linear proportional hazards
439 Cox model. In our approach, we did not use the propagation of standard statistical quantification
440 of the parameters' estimates uncertainty to evaluate the accuracy of the model predictions. Rather,
441 we relied on the RSF-outputted individual survival curves to sample virtual individuals and compute
442 prediction intervals.

443 A drawback of classical TK-OS studies is that they make use of the full observed kinetics to
444 predict overall survival, which can lead to time-dependent covariate bias⁵⁶ and limit their practical
445 applicability at bedside. We used individual-truncated data sets and found that kML was already
446 improving predictions over mBSL using data at 1.5 months, which corresponds to the first imag-
447 ing assessment of the treatment effect. At later times, stratification abilities increased to highly
448 significant levels (e.g., $HR = 5$ at 6.8 months).

449 A strength of our study is that we relied on well-curated data with high number of patients from
450 clinical trials. However, when extrapolating to other settings — earlier trial phases, real-world data
451 — limited number of patients might be available. Yet, we found that using only 60 patients to train
452 kML was sufficient to reach near-optimal performances.

453 Not only kML has value for personalized health care, but it revealed also useful for prediction of
454 a phase 3 trial using early on-study data. Our predictions compared favorably with previous work,
455 being able to predict the study's positive outcome from 25 weeks onwards, versus 40 weeks using
456 TK only¹⁹ and 60 weeks if relying on the observed data alone. Of note, in a recent evaluation based
457 on resampling the first-line NSCLC ATZ study IMpower150 to mimic small, short follow up early
458 Phase Ib studies, TK model-based metrics had better operating characteristics to predict Phase
459 III success compared with RECIST endpoints ORR and PFS⁵⁵. Extension of such results with the
460 addition of BKs is thus a promising line of research. In addition, kML, trained on ATZ data, yielded
461 excellent predictive abilities for the docetaxel (control) arm. This suggests that the relationships
462 between TK / BK and OS might be drug-independent. In turn, this opens future perspectives in
463 terms of testing kML on drugs with different mechanism of action, or combinations.

464 Further avenues of research comprise the development of integrative models from advanced
465 multi-modal data such as the one collected during the PIONeer clinical study (NCT03833440)^{57,58}
466 that include quantitative image analysis from multiplex immune-histochemistry staining of tumor
467 tissue, genomic and transcriptomic data, biological and clinical markers. In addition, mechanistic
468 modeling of quantitative and physiologically meaningful longitudinal data (immune-monitoring,
469 vasculo-monitoring, circulating DNA^{12,59-61}, soluble factors⁶², pharmacokinetics, TK and a large
470 number of BKs from either hematology or biochemistry) paves the way to an improved under-
471 standing and prediction of mechanisms of relapse to ICI⁶³. Furthermore, the predictive abilities of
472 kML — at the both individual and study levels — should be evaluated in model-based prospective
473 trials⁶⁴.

474 In conclusion, our study shows that integrating model-based on-treatment dynamic data from
475 routine biological markers shows great promise for both personalized health care and early pre-
476 diction of the outcome of late-phase trials during drug development.

477 References

- 478 1. Bray, F., Ferlay, J., *et al.* Global cancer statistics 2018: GLOBOCAN estimates of incidence and
479 mortality worldwide for 36 cancers in 185 countries. *CA: A Cancer Journal for Clinicians*, 394-
480 424. ISSN: 1542-4863. doi:[10.3322/caac.21492](https://doi.org/10.3322/caac.21492) (2018).

It is made available under a [CC-BY-NC-ND 4.0 International license](https://creativecommons.org/licenses/by-nc-nd/4.0/) .

- 481 2. Duma, N., Santana-Davila, R. & Molina, J. R. Non-Small Cell Lung Cancer: Epidemiology, Screen-
482 ing, Diagnosis, and Treatment. *Mayo Clinic Proceedings*, 1623–1640. ISSN: 0025-6196, 1942-
483 5546. doi:[10.1016/j.mayocp.2019.01.013](https://doi.org/10.1016/j.mayocp.2019.01.013) (2019).
- 484 3. Fehrenbacher, L., Spira, A., *et al.* Atezolizumab versus docetaxel for patients with previously
485 treated non-small-cell lung cancer (POPLAR): a multicentre, open-label, phase 2 randomised
486 controlled trial. *The Lancet*, 1837–1846. ISSN: 0140-6736, 1474-547X. doi:[10.1016/S0140-6736\(16\)](https://doi.org/10.1016/S0140-6736(16)00587-0)
487 [00587-0](https://doi.org/10.1016/S0140-6736(16)00587-0) (2016).
- 488 4. Grant, M. J., Herbst, R. S. & Goldberg, S. B. Selecting the optimal immunotherapy regimen in
489 driver-negative metastatic NSCLC. *Nature Reviews Clinical Oncology*, 625–644. ISSN: 1759-4782.
490 doi:[10.1038/s41571-021-00520-1](https://doi.org/10.1038/s41571-021-00520-1) (2021).
- 491 5. Camidge, D. R., Doebele, R. C. & Kerr, K. M. Comparing and contrasting predictive biomarkers
492 for immunotherapy and targeted therapy of NSCLC. *Nature Reviews Clinical Oncology*, 341–355.
493 ISSN: 1759-4782. doi:[10.1038/s41571-019-0173-9](https://doi.org/10.1038/s41571-019-0173-9) (2019).
- 494 6. Hutchinson, L. & Kirk, R. High drug attrition rates—where are we going wrong? *Nature Reviews*
495 *Clinical Oncology*, 189–190. ISSN: 1759-4782. doi:[10.1038/nrclinonc.2011.34](https://doi.org/10.1038/nrclinonc.2011.34) (2011).
- 496 7. Hua, T., Gao, Y., Zhang, R., Wei, Y. & Chen, F. Validating ORR and PFS as surrogate endpoints in
497 phase II and III clinical trials for NSCLC patients: difference exists in the strength of surrogacy
498 in various trial settings. *BMC Cancer*, 1022. ISSN: 1471-2407. doi:[10.1186/s12885-022-10046-z](https://doi.org/10.1186/s12885-022-10046-z)
499 (2022).
- 500 8. Rizvi, H., Sanchez-Vega, F., *et al.* Molecular Determinants of Response to Anti-Programmed
501 Cell Death (PD)-1 and Anti-Programmed Death-Ligand 1 (PD-L1) Blockade in Patients With
502 Non-Small-Cell Lung Cancer Profiled With Targeted Next-Generation Sequencing. *Journal of*
503 *Clinical Oncology*. doi:[10.1200/JCO.2017.75.3384](https://doi.org/10.1200/JCO.2017.75.3384) (2018).
- 504 9. Doroshov, D. B., Bhalla, S., *et al.* PD-L1 as a biomarker of response to immune-checkpoint
505 inhibitors. *Nature Reviews Clinical Oncology*, 345–362. ISSN: 1759-4782. doi:[10.1038/s41571-](https://doi.org/10.1038/s41571-021-00473-5)
506 [021-00473-5](https://doi.org/10.1038/s41571-021-00473-5) (2021).
- 507 10. So, W. V., Dejaridin, D., Rossmann, E. & Charo, J. Predictive biomarkers for PD-1/PD-L1 check-
508 point inhibitor response in NSCLC: an analysis of clinical trial and real-world data. *Journal for*
509 *Immunotherapy of Cancer*, e006464. ISSN: 2051-1426. doi:[10.1136/jitc-2022-006464](https://doi.org/10.1136/jitc-2022-006464) (2023).
- 510 11. Hellmann, M. D., Ciuleanu, T.-E., *et al.* Nivolumab plus Ipilimumab in Lung Cancer with a
511 High Tumor Mutational Burden. *New England Journal of Medicine*, 2093–2104. doi:[10.1056/](https://doi.org/10.1056/NEJMoa1801946)
512 [NEJMoa1801946](https://doi.org/10.1056/NEJMoa1801946) (2018).
- 513 12. Gandara, D. R., Paul, S. M., *et al.* Blood-based tumor mutational burden as a predictor of clini-
514 cal benefit in non-small-cell lung cancer patients treated with atezolizumab. *Nature Medicine*,
515 1441–1448. ISSN: 1546-170X. doi:[10.1038/s41591-018-0134-3](https://doi.org/10.1038/s41591-018-0134-3) (2018).
- 516 13. Cristescu, R., Mogg, R., *et al.* Pan-tumor genomic biomarkers for PD-1 checkpoint blockade-
517 based immunotherapy. *Science*, eaar3593. doi:[10.1126/science.aar3593](https://doi.org/10.1126/science.aar3593) (2018).
- 518 14. Sankar, K., Ye, J. C., *et al.* The role of biomarkers in personalized immunotherapy. *Biomarker*
519 *Research*, 32. ISSN: 2050-7771. doi:[10.1186/s40364-022-00378-0](https://doi.org/10.1186/s40364-022-00378-0) (2022).
- 520 15. Acosta, J. N., Falcone, G. J., Rajpurkar, P. & Topol, E. J. Multimodal biomedical AI. *Nature Medicine*,
521 1773–1784. ISSN: 1546-170X. doi:[10.1038/s41591-022-01981-2](https://doi.org/10.1038/s41591-022-01981-2) (2022).
- 522 16. Kurtz, D. M., Esfahani, M. S., *et al.* Dynamic Risk Profiling Using Serial Tumor Biomarkers for
523 Personalized Outcome Prediction. *Cell*, 699–713.e19. ISSN: 1097-4172. doi:[10.1016/j.cell.2019.](https://doi.org/10.1016/j.cell.2019.06.011)
524 [06.011](https://doi.org/10.1016/j.cell.2019.06.011) (2019).
- 525 17. Bonate, P. L. *Pharmacokinetic-Pharmacodynamic Modeling and Simulation* 2nd ed. 2011. ISBN:
526 978-1-4419-9484-4 (Springer-Verlag New York Inc., New York, 2011).

It is made available under a [CC-BY-NC-ND 4.0 International license](https://creativecommons.org/licenses/by-nc-nd/4.0/) .

- 527 18. Claret, L., Girard, P., *et al.* Model-based prediction of phase III overall survival in colorectal
528 cancer on the basis of phase II tumor dynamics. *J Clin Oncol*, 4103–4108. doi:[10.1200/JCO.](https://doi.org/10.1200/JCO.2008.21.0807)
529 [2008.21.0807](https://doi.org/10.1200/JCO.2008.21.0807) (2009).
- 530 19. Claret, L., Jin, J. Y., *et al.* A Model of Overall Survival Predicts Treatment Outcomes with Ate-
531 zolizumab versus Chemotherapy in Non-Small Cell Lung Cancer Based on Early Tumor Kinet-
532 ics. *Clin Cancer Res*, 3292–3298. doi:[10.1158/1078-0432.CCR-17-3662](https://doi.org/10.1158/1078-0432.CCR-17-3662) (2018).
- 533 20. Chan, P., Marchand, M., *et al.* Prediction of overall survival in patients across solid tumors fol-
534 lowing atezolizumab treatments: A tumor growth inhibition-overall survival modeling frame-
535 work. *CPT: pharmacometrics & systems pharmacology*, 1171–1182. ISSN: 2163-8306. doi:[10.1002/](https://doi.org/10.1002/psp4.12686)
536 [psp4.12686](https://doi.org/10.1002/psp4.12686) (2021).
- 537 21. Benzekry, S. Artificial intelligence and mechanistic modeling for clinical decision making in
538 oncology. *Clinical Pharmacology & Therapeutics*, 471–486. ISSN: 1532-6535. doi:[10.1002/cpt.](https://doi.org/10.1002/cpt.1951)
539 [1951](https://doi.org/10.1002/cpt.1951) (2020).
- 540 22. Chan, P., Zhou, X., *et al.* Application of Machine Learning for Tumor Growth Inhibition - Overall
541 Survival Modeling Platform. *CPT: pharmacometrics & systems pharmacology*, 59–66. ISSN: 2163-
542 8306. doi:[10.1002/psp4.12576](https://doi.org/10.1002/psp4.12576) (2021).
- 543 23. Ishwaran, H., Kogalur, U. B., Blackstone, E. H. & Lauer, M. S. Random survival forests. *The*
544 *Annals of Applied Statistics*, 841–860. ISSN: 1932-6157, 1941-7330. doi:[10.1214/08-](https://doi.org/10.1214/08-AOAS169)
545 [AOAS169](https://doi.org/10.1214/08-AOAS169) (2008).
- 546 24. Christodoulou, E., Ma, J., *et al.* A systematic review shows no performance benefit of machine
547 learning over logistic regression for clinical prediction models. *Journal of Clinical Epidemiology*,
548 12–22. ISSN: 0895-4356. doi:[10.1016/j.jclinepi.2019.02.004](https://doi.org/10.1016/j.jclinepi.2019.02.004) (2019).
- 549 25. Spigel, D. R., Chaft, J. E., *et al.* FIR: Efficacy, Safety, and Biomarker Analysis of a Phase II Open-
550 Label Study of Atezolizumab in PD-L1–Selected Patients With NSCLC. *Journal of Thoracic On-*
551 *cology*, 1733–1742. ISSN: 1556-0864. doi:[10.1016/j.jtho.2018.05.004](https://doi.org/10.1016/j.jtho.2018.05.004) (2018).
- 552 26. Peters, S., Gettinger, S., *et al.* Phase II Trial of Atezolizumab As First-Line or Subsequent Ther-
553 apy for Patients With Programmed Death-Ligand 1–Selected Advanced Non-Small-Cell Lung
554 Cancer (BIRCH). *Journal of Clinical Oncology: Official Journal of the American Society of Clinical*
555 *Oncology*, 2781–2789. ISSN: 1527-7755. doi:[10.1200/JCO.2016.71.9476](https://doi.org/10.1200/JCO.2016.71.9476) (2017).
- 556 27. Rittmeyer, A., Barlesi, F., *et al.* Atezolizumab versus docetaxel in patients with previously treated
557 non-small-cell lung cancer (OAK): a phase 3, open-label, multicentre randomised controlled
558 trial. *The Lancet*, 255–265. ISSN: 0140-6736, 1474-547X. doi:[10.1016/S0140-6736\(16\)32517-X](https://doi.org/10.1016/S0140-6736(16)32517-X)
559 (2017).
- 560 28. Bach, F. R. *Bolasso: model consistent Lasso estimation through the bootstrap* in (Association for
561 Computing Machinery, New York, NY, USA, 2008), 33–40. ISBN: 978-1-60558-205-4. doi:[10.](https://doi.org/10.1145/1390156.1390161)
562 [1145/1390156.1390161](https://doi.org/10.1145/1390156.1390161).
- 563 29. Lavielle, M. *Mixed Effects Models for the Population Approach* ISBN: 1-4822-2650-2 (CRC Press,
564 2014).
- 565 30. Delyon, B., Lavielle, M. & Moulines, E. Convergence of a stochastic approximation version of
566 the EM algorithm. *The Annals of Statistics*, 94–128. ISSN: 0090-5364, 2168-8966. doi:[10.1214/](https://doi.org/10.1214/aos/1018031103)
567 [aos/1018031103](https://doi.org/10.1214/aos/1018031103) (1999).
- 568 31. Lixoft. *Monolix version 2020R1*. Antony, France, 2020.
- 569 32. Stein, W. D., Figg, W. D., *et al.* Tumor growth rates derived from data for patients in a clinical
570 trial correlate strongly with patient survival: a novel strategy for evaluation of clinical trial data.
571 *The Oncologist*, 1046–1054. doi:[10.1634/theoncologist.2008-0075](https://doi.org/10.1634/theoncologist.2008-0075) (2008).
- 572 33. Delattre, M., Lavielle, M. & Poursat, M.-A. A note on BIC in mixed-effects models. *Electronic*
573 *Journal of Statistics*, 456–475. ISSN: 1935-7524, 1935-7524. doi:[10.1214/14-EJS890](https://doi.org/10.1214/14-EJS890) (2014).

- 574 34. Cox, D. R. Regression Models and Life-Tables. *Journal of the Royal Statistical Society. Series B*
575 *(Methodological)*, 187–220. ISSN: 0035-9246 (1972).
- 576 35. Chen, T. & Guestrin, C. *XGBoost: A Scalable Tree Boosting System in Proceedings of the 22nd*
577 *ACM SIGKDD International Conference on Knowledge Discovery and Data Mining* (Association for
578 Computing Machinery, San Francisco, California, USA, 2016), 785–794. ISBN: 9781450342322.
579 doi:[10.1145/2939672.2939785](https://doi.org/10.1145/2939672.2939785).
- 580 36. Cawley, G. C. & Talbot, N. L. C. On over-fitting in model selection and subsequent selection
581 bias in performance evaluation. *Journal of Machine Learning Research*, 2079–2107 (2010).
- 582 37. Harrell, F. E., Califf, R. M., Pryor, D. B., Lee, K. L. & Rosati, R. A. Evaluating the yield of medical
583 tests. *JAMA*, 2543–2546. ISSN: 0098-7484 (1982).
- 584 38. Harrell, F. E. Hmisc: Harrell miscellaneous. *R package*. [https://CRAN.R-project.org/package=](https://CRAN.R-project.org/package=Hmisc)
585 [Hmisc](https://CRAN.R-project.org/package=Hmisc) (2022).
- 586 39. Heagerty, P. J., Lumley, T. & Pepe, M. S. Time-dependent ROC curves for censored survival
587 data and a diagnostic marker. *Biometrics*, 337–344. ISSN: 0006-341X. doi:[10.1111/j.0006-341x.](https://doi.org/10.1111/j.0006-341x.2000.00337.x)
588 [2000.00337.x](https://doi.org/10.1111/j.0006-341x.2000.00337.x) (2000).
- 589 40. Heagerty, P. J. & Saha-Chaudhuri, p. b. P. *survivalROC: Time-dependent ROC curve estimation*
590 *from censored survival data* tech. rep. (2013). <https://CRAN.R-project.org/package=survivalROC>.
- 591 41. Tibshirani, R. Regression Shrinkage and Selection via the Lasso. *Journal of the Royal Statistical*
592 *Society. Series B (Methodological)*, 267–288. ISSN: 0035-9246 (1996).
- 593 42. Eisenhauer, E. A., Therasse, P., *et al.* New response evaluation criteria in solid tumours: Revised
594 RECIST guideline (version 1.1). *European Journal of Cancer. Response assessment in solid tumours*
595 *(RECIST): Version 1.1 and supporting papers* 228–247. ISSN: 0959-8049. doi:[10.1016/j.ejca.2008.](https://doi.org/10.1016/j.ejca.2008.10.026)
596 [10.026](https://doi.org/10.1016/j.ejca.2008.10.026) (2009).
- 597 43. Benzekry, S., Grangeon, M., *et al.* Machine Learning for Prediction of Immunotherapy Efficacy
598 in Non-Small Cell Lung Cancer from Simple Clinical and Biological Data. *Cancers*, 6210. doi:[10.](https://doi.org/10.3390/cancers13246210)
599 [3390/cancers13246210](https://doi.org/10.3390/cancers13246210) (2021).
- 600 44. Havel, J. J., Chowell, D. & Chan, T. A. The evolving landscape of biomarkers for checkpoint in-
601 hibitor immunotherapy. *Nature Reviews Cancer*, 133–150. ISSN: 1474-1768. doi:[10.1038/s41568-](https://doi.org/10.1038/s41568-019-0116-x)
602 [019-0116-x](https://doi.org/10.1038/s41568-019-0116-x) (2019).
- 603 45. Blank, C. U., Haanen, J. B., Ribas, A. & Schumacher, T. N. The “cancer immunogram”. *Science*,
604 658–660. doi:[10.1126/science.aaf2834](https://doi.org/10.1126/science.aaf2834) (2016).
- 605 46. Peters, S., Dziadziuszko, R., *et al.* Atezolizumab versus chemotherapy in advanced or metastatic
606 NSCLC with high blood-based tumor mutational burden: primary analysis of BFAST cohort C
607 randomized phase 3 trial. *Nature Medicine*, 1831–1839. ISSN: 1546-170X. doi:[10.1038/s41591-](https://doi.org/10.1038/s41591-022-01933-w)
608 [022-01933-w](https://doi.org/10.1038/s41591-022-01933-w) (2022).
- 609 47. Liu, Y., Wang, B., Tian, H. & Hsu, J. C. Rejoinder for discussions on correct and logical causal
610 inference for binary and time-to-event outcomes in randomized controlled trials. *Biometrical*
611 *Journal*, 246–255. ISSN: 1521-4036. doi:[10.1002/bimj.202100089](https://doi.org/10.1002/bimj.202100089) (2022).
- 612 48. Soyano, A. E., Dholaria, B., *et al.* Peripheral blood biomarkers correlate with outcomes in ad-
613 vanced non-small cell lung Cancer patients treated with anti-PD-1 antibodies. *Journal for Im-*
614 *muno-therapy of Cancer*, 129. ISSN: 2051-1426. doi:[10.1186/s40425-018-0447-2](https://doi.org/10.1186/s40425-018-0447-2) (2018).
- 615 49. Diem, S., Schmid, S., *et al.* Neutrophil-to-Lymphocyte ratio (NLR) and Platelet-to-Lymphocyte
616 ratio (PLR) as prognostic markers in patients with non-small cell lung cancer (NSCLC) treated
617 with nivolumab. *Lung Cancer (Amsterdam, Netherlands)*, 176–181. ISSN: 1872-8332. doi:[10.1016/](https://doi.org/10.1016/j.lungcan.2017.07.024)
618 [j.lungcan.2017.07.024](https://doi.org/10.1016/j.lungcan.2017.07.024) (2017).

It is made available under a [CC-BY-NC-ND 4.0 International license](https://creativecommons.org/licenses/by-nc-nd/4.0/) .

- 619 50. Peng, L., Wang, Y., *et al.* Peripheral blood markers predictive of outcome and immune-related
620 adverse events in advanced non-small cell lung cancer treated with PD-1 inhibitors. *Cancer*
621 *immunology, immunotherapy: CII*, 1813–1822. ISSN: 1432-0851. doi:[10.1007/s00262-020-02585-](https://doi.org/10.1007/s00262-020-02585-w)
622 [w](https://doi.org/10.1007/s00262-020-02585-w) (2020).
- 623 51. Becker, T., Weberpals, J., *et al.* An enhanced prognostic score for overall survival of patients
624 with cancer derived from a large real-world cohort. *Annals of Oncology*, 1561–1568. ISSN: 0923-
625 7534. doi:[10.1016/j.annonc.2020.07.013](https://doi.org/10.1016/j.annonc.2020.07.013) (2020).
- 626 52. Gavrillov, S., Zhudenkova, K., *et al.* Longitudinal Tumor Size and Neutrophil-to-Lymphocyte Ratio
627 Are Prognostic Biomarkers for Overall Survival in Patients With Advanced Non-Small Cell Lung
628 Cancer Treated With Durvalumab. *CPT: pharmacometrics & systems pharmacology*, 67–74. ISSN:
629 2163-8306. doi:[10.1002/psp4.12578](https://doi.org/10.1002/psp4.12578) (2021).
- 630 53. Yang, J.-R., Xu, J.-Y., *et al.* Post-diagnostic C-reactive protein and albumin predict survival in
631 Chinese patients with non-small cell lung cancer: a prospective cohort study. *Scientific Reports*,
632 8143. ISSN: 2045-2322. doi:[10.1038/s41598-019-44653-x](https://doi.org/10.1038/s41598-019-44653-x) (2019).
- 633 54. Bruni, D., Angell, H. K. & Galon, J. The immune contexture and Immunoscore in cancer prog-
634 nosis and therapeutic efficacy. *Nature Reviews Cancer*, 662–680. ISSN: 1474-1768. doi:[10.1038/](https://doi.org/10.1038/s41568-020-0285-7)
635 [s41568-020-0285-7](https://doi.org/10.1038/s41568-020-0285-7) (2020).
- 636 55. Bruno, R., Marchand, M., *et al.* Tumor Dynamic Model-Based Decision Support for Phase Ib/II
637 Combination Studies: A Retrospective Assessment Based on Resampling of the Phase III Study
638 IMpower150. *Clinical Cancer Research*, OF1–OF9. ISSN: 1078-0432. doi:[10.1158/1078-0432.CCR-](https://doi.org/10.1158/1078-0432.CCR-22-2323)
639 [22-2323](https://doi.org/10.1158/1078-0432.CCR-22-2323) (2023).
- 640 56. Desmée, S., Mentré, F., Veyrat-Follet, C. & Guedj, J. Nonlinear Mixed-Effect Models for Prostate-
641 Specific Antigen Kinetics and Link with Survival in the Context of Metastatic Prostate Cancer:
642 a Comparison by Simulation of Two-Stage and Joint Approaches. *The AAPS Journal*, 691–699.
643 ISSN: 1550-7416. doi:[10.1208/s12248-015-9745-5](https://doi.org/10.1208/s12248-015-9745-5) (2015).
- 644 57. Greillier, L., Monville, F., *et al.* Abstract LB120: Comprehensive biomarkers analysis to explain
645 resistances to PD1-L1 ICIs: The precision immuno-oncology for advanced non-small cell lung
646 cancer (PIONeeR) trial. *Cancer Research*, LB120. ISSN: 0008-5472. doi:[10.1158/1538-7445.](https://doi.org/10.1158/1538-7445.AM2022-LB120)
647 [AM2022-LB120](https://doi.org/10.1158/1538-7445.AM2022-LB120) (2022).
- 648 58. Barlesi, F., Monville, F., *et al.* Comprehensive biomarkers (BMs) analysis to predict efficacy of
649 PD1-L1 immune checkpoint inhibitors (ICIs) in combination with chemotherapy: a subgroup
650 analysis of the Precision Immuno-Oncology for advanced Non-Small Cell Lung CancER (PIO-
651 NeeR) trial. *Annals of Oncology*. doi:[10.1016/j.annonc.2022.07.013](https://doi.org/10.1016/j.annonc.2022.07.013) (2022).
- 652 59. Assaf, Z. J. F., Zou, W., *et al.* A longitudinal circulating tumor DNA-based model associated with
653 survival in metastatic non-small-cell lung cancer. *Nature Medicine*, 859–868. ISSN: 1546-170X.
654 doi:[10.1038/s41591-023-02226-6](https://doi.org/10.1038/s41591-023-02226-6) (2023).
- 655 60. Nabet, B. Y., Esfahani, M. S., *et al.* Noninvasive Early Identification of Therapeutic Benefit from
656 Immune Checkpoint Inhibition. *Cell*, 363–376.e13. ISSN: 1097-4172. doi:[10.1016/j.cell.2020.09.](https://doi.org/10.1016/j.cell.2020.09.001)
657 [001](https://doi.org/10.1016/j.cell.2020.09.001) (2020).
- 658 61. Cabel, L., Proud'hon, C., *et al.* Clinical potential of circulating tumour DNA in patients receiv-
659 ing anticancer immunotherapy. *Nature Reviews. Clinical Oncology*, 639–650. ISSN: 1759-4782.
660 doi:[10.1038/s41571-018-0074-3](https://doi.org/10.1038/s41571-018-0074-3) (2018).
- 661 62. Barrera, L., Montes-Servín, E., *et al.* Cytokine profile determined by data-mining analysis set
662 into clusters of non-small-cell lung cancer patients according to prognosis. *Annals of Oncology:*
663 *Official Journal of the European Society for Medical Oncology*, 428–435. ISSN: 1569-8041. doi:[10.](https://doi.org/10.1093/annonc/mdu549)
664 [1093/annonc/mdu549](https://doi.org/10.1093/annonc/mdu549) (2015).

It is made available under a [CC-BY-NC-ND 4.0 International license](#) .

- 665 63. Ciccolini, J., Benzekry, S. & Barlesi, F. Deciphering the response and resistance to immune-
666 checkpoint inhibitors in lung cancer with artificial intelligence-based analysis: when PIONeer
667 meets QUANTIC. *British Journal of Cancer*, 1–2. ISSN: 1532-1827. doi:[10.1038/s41416-020-0918-3](https://doi.org/10.1038/s41416-020-0918-3)
668 (2020).
- 669 64. Ciccolini, J., Barbolosi, D., André, N., Barlesi, F. & Benzekry, S. Mechanistic Learning for Com-
670 binatorial Strategies With Immuno-oncology Drugs: Can Model-Informed Designs Help Inves-
671 tigators? *JCO Precision Oncology*, 486–491. doi:[10.1200/PO.19.00381](https://doi.org/10.1200/PO.19.00381) (2020).

672 **Appendix 1**

673

Supplementary figures

Study	Description	Population	N
FIR GO28625	Phase 2 study for the efficacy and safety of ATZ in advanced NSCLC	PD-L1 positive locally advanced or metastatic NSCLC (lines 1 and 2+)	133
POPLAR GO28753	Phase 2 randomised controlled trial of ATZ versus docetaxel in NSCLC	Locally advanced or metastatic NSCLC who failed platinum therapy (line 2)	134
BIRCH GO28754	Phase 2 study of ATZ in advanced or metastatic NSCLC	Locally advanced or metastatic NSCLC (lines 1, 2 or 3)	595
Train			862
Test - OAK GO28915	Phase 3 RCT of ATZ versus docetaxel (DTX) in patients with previously treated NSCLC	Stage IIIB or IV, previously chemo treated	553
Train + Test			1415

Four monotherapy studies of atezolizumab in advanced NSCLC. NSCLC: Non-Small Cell Lung Cancer; p = number of parameters, N: number of patients treated with atezolizumab (patients from French centers were excluded for legal reasons (N=118)); In total, data from 1074 patients from OAK were used as Test set (553 from the ATZ arm, 521 from the DTX arm); PD: Pharmacodynamic; SLD: Sum of the Largest Diameters. CRP: C Reactive Protein; LDH: Lactate Dehydrogenase.

1

674

676

Appendix 1—figure 1. Train and test data sets

Characteristic	Total, N = 1415 ¹	FIR, N = 133 ¹	POPLAR, N = 134 ¹	BIRCH, N = 595 ¹	OAK, N = 553 ¹	p-value ²
Age	64 (57, 70)	67 (60, 73)	62 (55, 69)	65 (57, 71)	64 (57, 70)	<0.001
Sex						0.3
Female	568 (40%)	57 (43%)	47 (35%)	251 (42%)	213 (39%)	
Male	847 (60%)	76 (57%)	87 (65%)	344 (58%)	340 (61%)	
Weight	72 (61, 82)	70 (60, 83)	73 (63, 84)	72 (61, 82)	71 (60, 82)	0.3
BMI	24.9 (22.1, 28.1)	24.8 (21.9, 27.6)	25.2 (22.8, 28.7)	25.0 (22.1, 28.2)	24.7 (22.0, 28.1)	0.4
Unknown	65	8	5	30	22	
Race						<0.001
Asian	228 (16%)	6 (4.5%)	23 (17%)	77 (13%)	122 (22%)	
Others, unknown or missing	73 (5.2%)	9 (6.8%)	9 (6.7%)	23 (3.9%)	32 (5.8%)	
White	1,114 (79%)	118 (89%)	102 (76%)	495 (83%)	399 (72%)	
Smoking history						0.13
Current	171 (12%)	18 (14%)	22 (16%)	60 (10%)	71 (13%)	
Never	248 (18%)	16 (12%)	27 (20%)	102 (17%)	103 (19%)	
Previous	996 (70%)	99 (74%)	85 (63%)	433 (73%)	379 (69%)	

Characteristic	Total, N = 1415 ¹	FIR, N = 133 ¹	POPLAR, N = 134 ¹	BIRCH, N = 595 ¹	OAK, N = 553 ¹	p-value ²
Heart rate	81 (71, 92)	80 (70, 94)	84 (74, 96)	80 (70, 90)	81 (72, 93)	0.049
Systolic blood pressure	122 (111, 133)	122 (113, 132)	122 (112, 131)	120 (110, 133)	123 (113, 135)	0.13

¹Median (IQR); n (%)

²Kruskal-Wallis rank sum test; Pearson's Chi-squared test

677

679

Appendix 1—figure 2. Patient characteristics: demographics and clinics

It is made available under a [CC-BY-NC-ND 4.0 International license](https://creativecommons.org/licenses/by-nc-nd/4.0/).

Characteristic	Total, N = 1415 ¹	FIR, N = 133 ¹	POPLAR, N = 134 ¹	BIRCH, N = 595 ¹	OAK, N = 553 ¹	p-value ²
Disease type						0.4
Locally advanced	77 (5.4%)	3 (2.3%)	8 (6.0%)	32 (5.4%)	34 (6.1%)	
Metastatic	1,338 (95%)	130 (98%)	126 (94%)	563 (95%)	519 (94%)	
Line						<0.001
≥2	1,255 (89%)	102 (77%)	134 (100%)	466 (78%)	553 (100%)	
1	160 (11%)	31 (23%)	0 (0%)	129 (22%)	0 (0%)	
Histology						<0.001
Non-squamous	1,016 (74%)	95 (100%)	87 (65%)	427 (72%)	407 (74%)	
Squamous	361 (26%)	0 (0%)	47 (35%)	168 (28%)	146 (26%)	
Unknown	38	38	0	0	0	
Stage						<0.001
I	123 (8.9%)	11 (8.7%)	4 (3.0%)	73 (12%)	35 (6.5%)	
II	140 (10%)	11 (8.7%)	9 (6.8%)	73 (12%)	47 (8.7%)	
III	367 (27%)	30 (24%)	37 (28%)	165 (28%)	135 (25%)	
IV	753 (54%)	75 (59%)	82 (62%)	273 (47%)	323 (60%)	
Unknown	32	6	2	11	13	
Number of metastases						0.4
1	386 (28%)	35 (27%)	34 (26%)	158 (27%)	159 (29%)	
2	655 (48%)	55 (42%)	61 (47%)	289 (50%)	250 (46%)	
3	334 (24%)	41 (31%)	34 (26%)	128 (22%)	131 (24%)	
Unknown	40	2	5	20	13	
Liver metastases	272 (19%)	29 (22%)	33 (25%)	105 (18%)	105 (19%)	0.3
Number of met. loc.						0.3
Four sites	70 (4.9%)	13 (9.8%)	6 (4.5%)	27 (4.5%)	24 (4.3%)	
One site	426 (30%)	37 (28%)	39 (29%)	178 (30%)	172 (31%)	
Three sites	264 (19%)	28 (21%)	28 (21%)	101 (17%)	107 (19%)	
Two sites	655 (48%)	55 (41%)	61 (46%)	289 (49%)	250 (45%)	
Tumor size	59 (43, 95)	59 (57, 59)	70 (43, 107)	60 (37, 96)	70 (43, 102)	0.001

¹n (%); Median (IQR)

²Pearson's Chi-squared test; Kruskal-Wallis rank sum test

680

682

Appendix 1—figure 3. Patient characteristics: disease

Characteristic	Total, N = 1415 ¹	FIR, N = 133 ¹	POPLAR, N = 134 ¹	BIRCH, N = 595 ¹	OAK, N = 553 ¹	p-value ²
PD-L1 tumor cells						<0.001
0	606 (43%)	4 (3.0%)	40 (30%)	212 (36%)	350 (64%)	
1	209 (15%)	21 (16%)	56 (42%)	69 (12%)	63 (11%)	
2	381 (27%)	105 (79%)	37 (28%)	160 (27%)	79 (14%)	
3	217 (15%)	3 (2.3%)	1 (0.7%)	154 (26%)	59 (11%)	
Unknown	2	0	0	0	2	
PD-L1 immune cells						<0.001
0	252 (18%)	3 (2.3%)	40 (30%)	16 (2.7%)	193 (35%)	
1	398 (28%)	5 (3.8%)	56 (42%)	122 (21%)	215 (39%)	
2	439 (31%)	25 (19%)	19 (14%)	297 (50%)	98 (18%)	
3	322 (23%)	99 (75%)	19 (14%)	159 (27%)	45 (8.2%)	
Unknown	4	1	0	1	2	
ECOG						0.6
Status 0	505 (36%)	42 (32%)	44 (33%)	215 (36%)	204 (37%)	
Status 1 or 2	909 (64%)	90 (68%)	90 (67%)	380 (64%)	349 (63%)	
Unknown	1	1	0	0	0	

¹n (%)

²Pearson's Chi-squared test

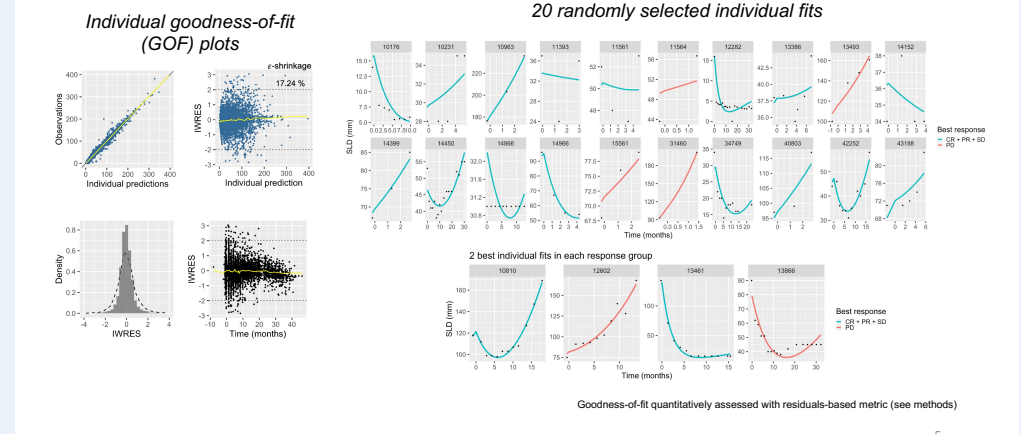
683

685

Appendix 1—figure 4. Patient characteristics: PD-L1 and ECOG

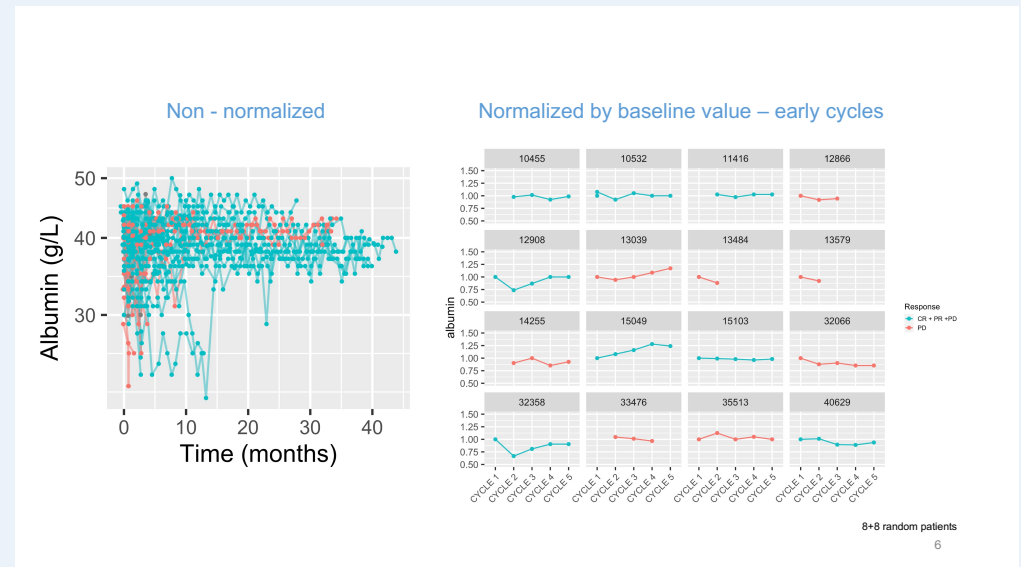
It is made available under a [CC-BY-NC-ND 4.0 International license](https://creativecommons.org/licenses/by-nc-nd/4.0/).

686
688



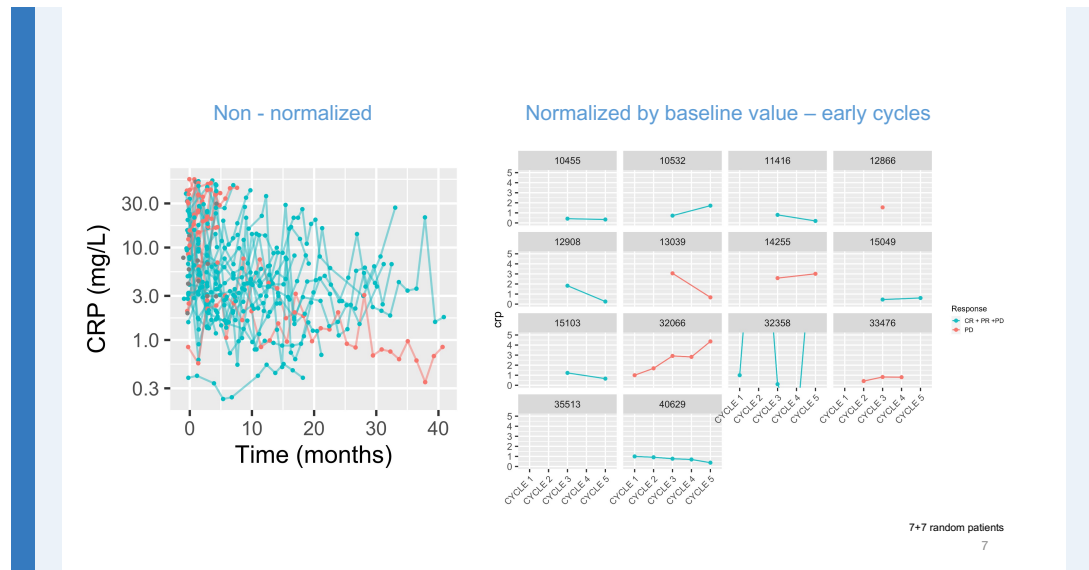
Appendix 1—figure 5. TK modeling goodness-of-fit

689
690



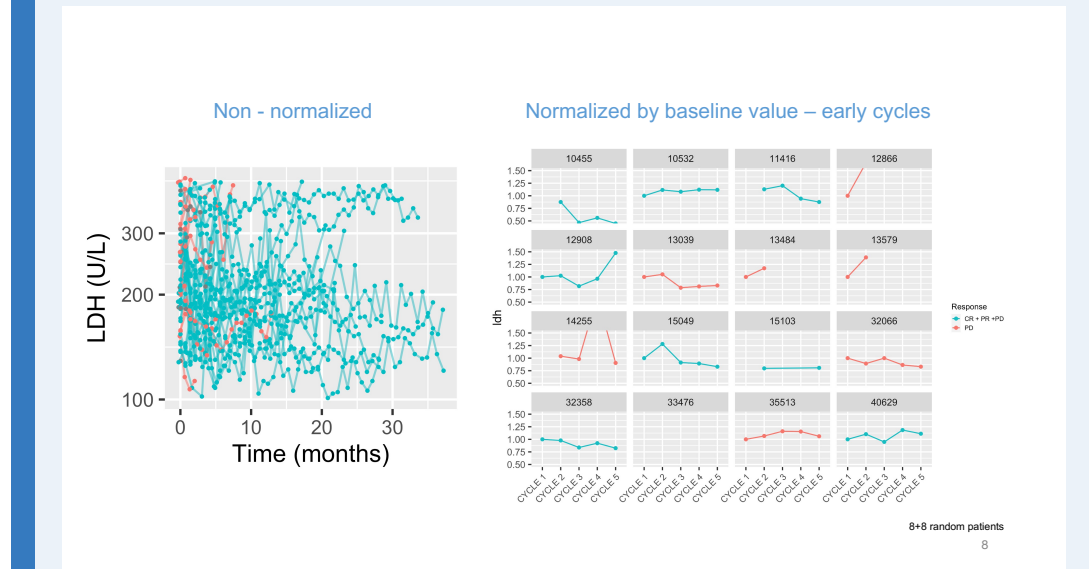
Appendix 1—figure 6. Examples of longitudinal kinetics: Albumin

It is made available under a [CC-BY-NC-ND 4.0 International license](https://creativecommons.org/licenses/by-nc-nd/4.0/).



692
694

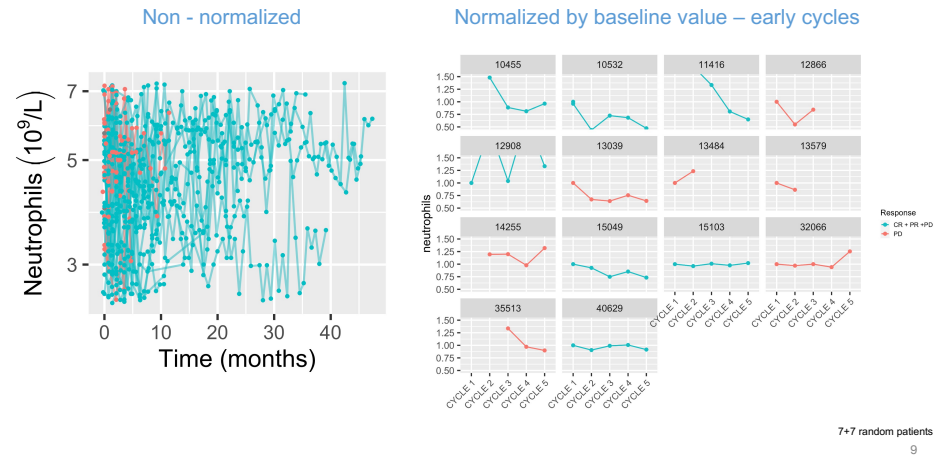
Appendix 1—figure 7. Examples of longitudinal kinetics: CRP



695
696

Appendix 1—figure 8. Examples of longitudinal kinetics: LDH

It is made available under a [CC-BY-NC-ND 4.0 International license](https://creativecommons.org/licenses/by-nc-nd/4.0/).



698
700

Appendix 1—figure 9. Examples of longitudinal kinetics: Neutrophils

Model	Albumin		CRP		LDH		Neutrophils	
	BICc	b	BICc	b	BICc	b	BICc	b
Double-exponential	48,395	0.058	28,764	0.21	39,886	0.56	102,449	0.14
Hyperbolic	48,007	0.056	29,712	0.22	40,915	0.62	102,943	0.14
Linear	49,436	0.063	30,020	0.23	42,462	0.70	105,193	0.17
Constant	49,724	0.065	31,332	0.25	42,982	0.74	106,249	0.18

Corrected Bayesian Information Criterion (BICc) for four empirical kinetic models of BK. b : standard deviation of the proportional error model

701
703

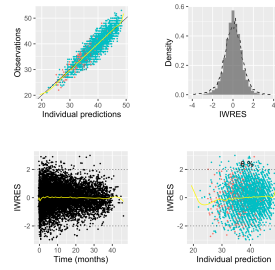
Appendix 1—figure 10. Goodness-of-fit metrics of dynamic BK models

10

It is made available under a [CC-BY-NC-ND 4.0 International license](https://creativecommons.org/licenses/by-nc-nd/4.0/).

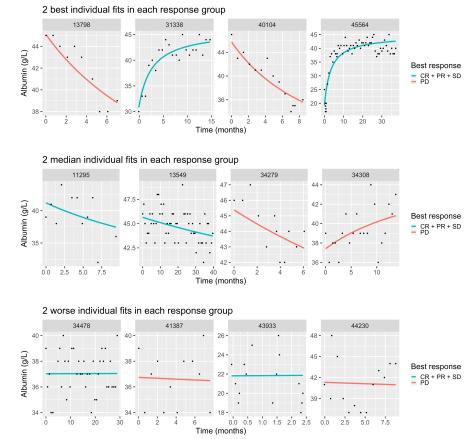
704
706

Individual residuals



- ⇒ Good description of individual kinetics
- ⇒ No sign of model misspecification at individual level

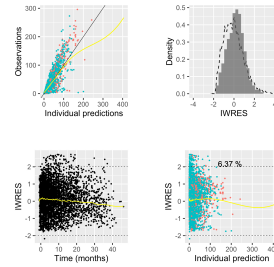
Individual fits in patients with at least 10 data points



Appendix 1—figure 11. Albumin: hyperbolic individual fits

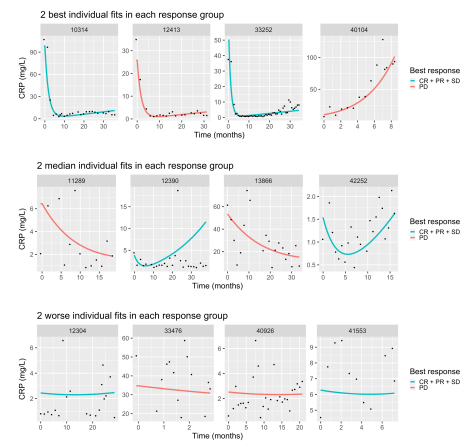
707
709

Individual residuals



- ⇒ Globally, several individuals not adequately fitted
- ⇒ Nevertheless, some patients have very accurate fits
- ⇒ Some trend of the model to underestimation
- ⇒ Distribution of IWRES remains close to gaussian

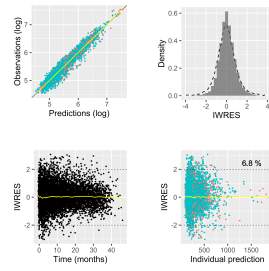
Individual fits in patients with at least 10 data points



Appendix 1—figure 12. CRP: dexr individual fits

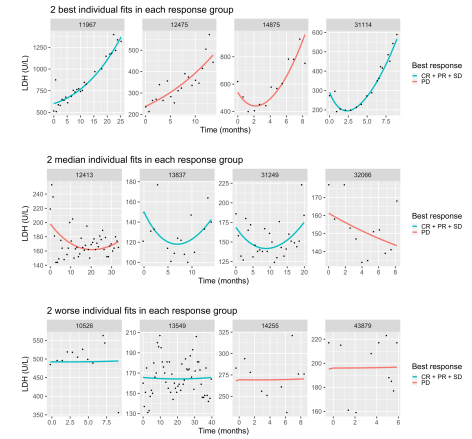
710
712

Individual residuals



- ⇒ Very good description of individual kinetics
- ⇒ No sign of model misspecification at individual level

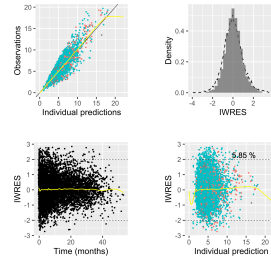
Individual fits in patients with at least 10 data points



Appendix 1—figure 13. LDH: dex individual fits

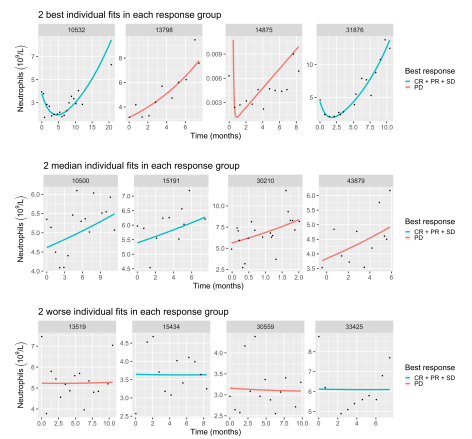
713
715

Individual residuals



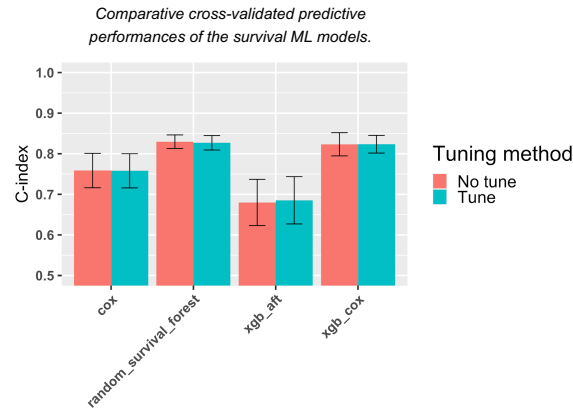
- ⇒ Moderate description of individual kinetics
- ⇒ No major sign of model misspecification at individual level

Individual fits in patients with at least 10 data points



Appendix 1—figure 14. Neutrophils: dex individual fits

It is made available under a [CC-BY-NC-ND 4.0 International license](https://creativecommons.org/licenses/by-nc-nd/4.0/).

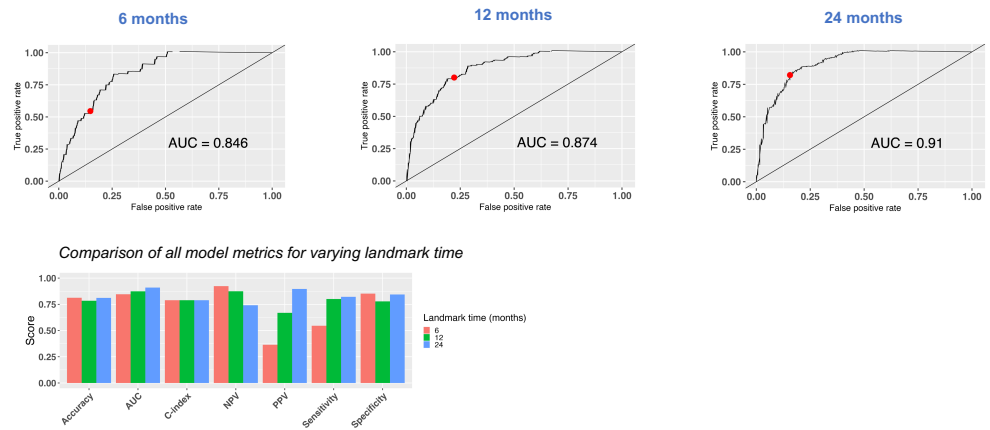


Note: 10-fold cross-validation on FIR, BIRCH and POPLAR (train data set) – performances using all features

15

716
718

Appendix 1—figure 15. Comparison of ML algorithms and tuning methods

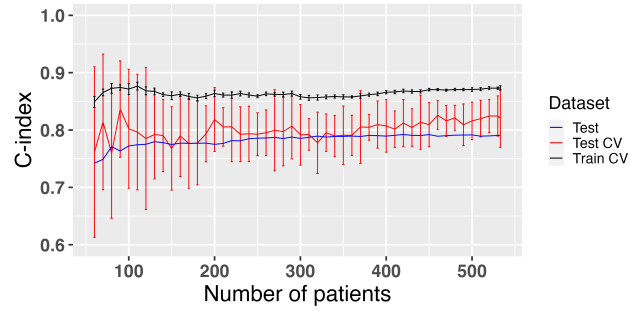


16

719
720

Appendix 1—figure 16. ROC curves for variables landmark times (test set - OAK)

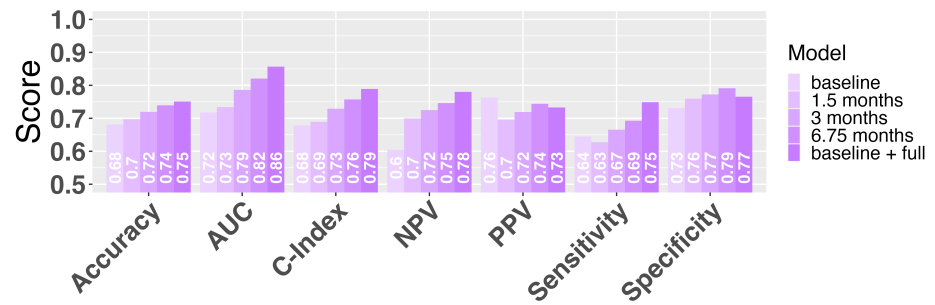
It is made available under a [CC-BY-NC-ND 4.0 International license](https://creativecommons.org/licenses/by-nc-nd/4.0/).



17

722
724

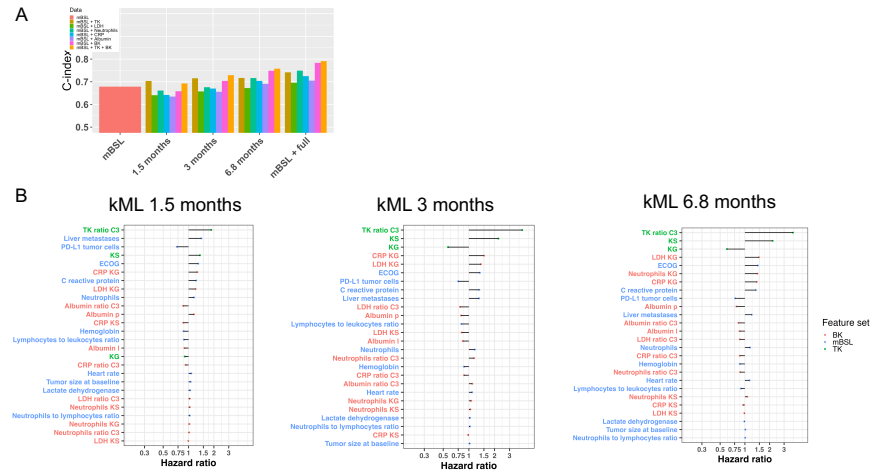
Appendix 1—figure 17. Learning curve



725
726

Appendix 1—figure 18. Additional value of NLME to baseline for multiple metrics

It is made available under a [CC-BY-NC-ND 4.0 International license](https://creativecommons.org/licenses/by-nc-nd/4.0/).



728
730

Appendix 1—figure 19. kML models using only single kinetic markers